Exergoeconomic optimization of a shell-and-tube heat exchanger

Muhammad Ahmad Jamil[a,b]♣, Talha S. Goraya[a], Muhammad Wakil Shahzad[b], and Syed M. Zubair[c]♣

[a]Department of Mechanical Engineering, Khwaja Fareed University of Engineering and Information Technology, Rahim Yar Khan, Pakistan
[b]Mechanical & Construction Engineering Department, Northumbria University, Newcastle Upon Tyne, UK
[c]Mechanical Engineering Department, KFUPM Box # 1474 King Fahd University of Petroleum & Minerals, Dhahran 31261, Saudi Arabia

ABSTRACT

The paper presents an economic optimization of STHX with two commonly adopted (i.e., Kern and Bell-Delaware) and one rarely explored (i.e., Wills-Johnston) methods. A detailed numerical code concerning thermal, hydraulic, exergy, and economic analysis of STHX is developed for all three methods. Normalized sensitivity analysis, parametric study, and Genetic Algorithm are used to ascertain the most influential parameters and optimize the total cost. It is observed that the calculations made using the Wills-Johnston method were reasonably close to the Bell-Delaware method. While the Kern method showed a significant deviation in the shell side calculations because of the several assumptions in this method. The parametric analysis showed that increasing the mass flow rate and the number of baffles increased the operating cost because of an exponential increase in the pressure drops. Finally, the optimization reduced the heat transfer area by ~26.4%, capital cost by ~20%, operational cost by ~50%, total cost by ~22%, and the stream cost by ~21%.

Keywords: shell and tube heat exchanger; exergoeconomic optimization; Kern; Bell-Delaware; Wills-Johnston; Genetic Algorithm

♣ Corresponding author; e-mail: ahmad.jamil@kfueit.edu.pk (M.A. Jamil); smzubair@kfpm.edu.sa (S.M. Zubair);

25 **GRAPHICAL ABSTRACT**

26

27

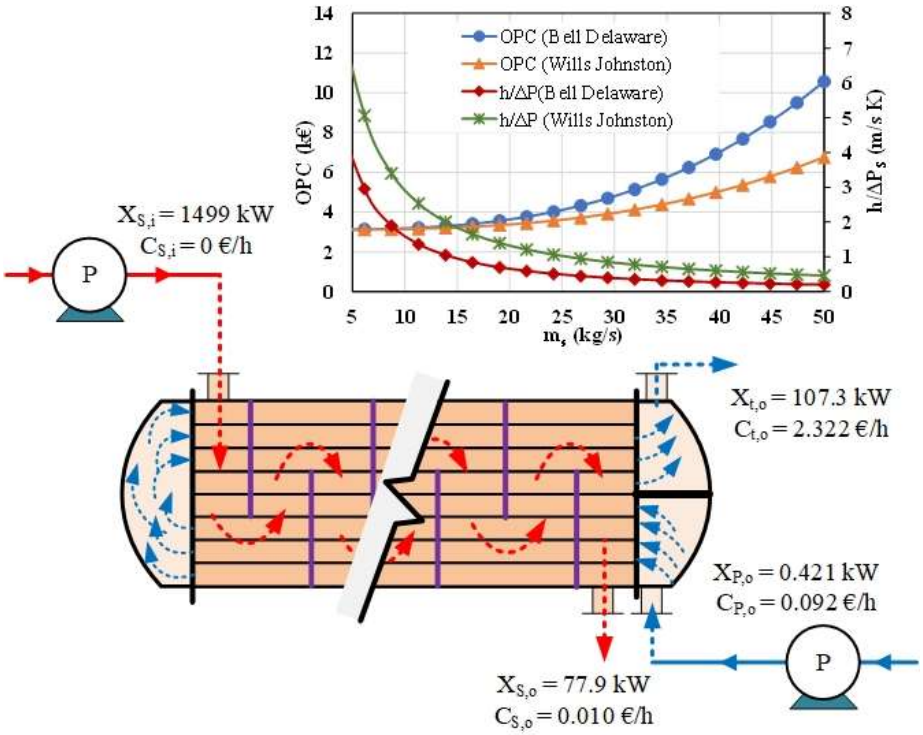

28

29

1. Introduction

The economic optimization of energy conversion systems is becoming inevitable with growing energy demands, cost-effective design, sustainable developments, and hikes in energy prices [1–3]. Heat exchangers not only play an important role as an integral part of almost every energy conversion system but also help to improve system efficiency by recovering heat from waste streams [4,5]. The most commonly used heat exchangers include shell-and-tube heat exchangers (STHX), gasketed plate heat exchangers, double pipe heat exchangers, and finned surface heat exchangers [6,7]. Among all, the STHXs are of particular importance and cover ~35-40% of the market because of larger heat transfer capabilities and high-pressure applications [8,9]. Therefore, the performance of these heat exchangers has been investigated extensively under varied operating conditions [10,11].

However, most of these studies are focused on improving thermal-hydraulic performance by varying geometric parameters such as baffle spacing, baffle orientation, the number of tubes, tube diameter. For instance, Jozaei et al. [12] reported that thermal-hydraulic performance decreases with increasing baffle spacing and suggested the range from 4 to 12 inches. Similarly, Abdelkader and Zubair [13] reported an increase in thermal-hydraulic performance with an increasing number of baffles. Furthermore, they reported that the heat transfer coefficient increased at a high rate when the square tube layout is used. Gao et al. [14] analyzed the effect of helical angle for discontinuous helical baffle STHX and reported that the helical angle with 40° provides the best comprehensive performance. Similarly, Abdelkader et al. [15] reported that the performance of a helical baffle HX decreased after the helix angle exceeded 42°.

Recently, researchers and industrialists have realized that STHXs optimization from a monetary viewpoint is also important together with conventional performance and design analysis [16,17]. It will have a great impact on overall system cost as they form a major portion of initial capital. For this purpose, various numerical approaches have been developed and used by the research community to minimize the total cost (C_{total}) of STHXs, which include capital (CAPC) and operational cost (OPC). For example, Selbas et al. [18] used Genetic Algorithm to minimize the heat transfer area and cost. They reported that the GA can achieve significant improvement in the design compared to the conventional methods. Segundo et al. [19] proposed a falcon optimization algorithm and reported that the cost is reduced by 57.8% and effectiveness is increased by 10% for case 2. A critical review of some other recent studies conducted in this regard

is presented in Table 1. It is important to notice that, most of these studies have reported a considerable improvement in the performance of STHX by optimizing the objective functions such as effectiveness, heat transfer coefficients, pressure, and cost. However, there is another STHX analysis method "Flow Stream Analysis" or the Wills-Johnston method that has not been critically explored. Besides, most optimization techniques adopted in the studies presented in Table 1 are computationally expensive and require adequate knowledge and computational capacity. Therefore, analysis of STHX as an integral part of systems with multiple components e.g., power plants, desalination systems, cogeneration systems, etc. is not economical due to the combinatory effects of design variables and objective functions.

On the other hand, exergoeconomic analysis, a combined application of thermodynamics and economic analyses, is an important tool for thermal systems analysis [20]. It calculates the exergy and economic values of each fluid stream as it enters or leaves any component using capital and operational expenses, thus predicting the local product stream cost [21]. The product stream is defined based on a primary function of the equipment, e.g., for a pump, it is pressurized water; for a compressor, it is compressed vapor, and for an HX, it is hot/cold stream. Besides the calculation of local product cost, the analysis can also conduct design improvements and malfunctioning diagnosis [22]. This tool has already been used to improve systems like refrigeration [23], desalination [24–26], and heat recovery units [27]. It should be noted that a thorough exergo-economic design and optimization study of SHTX, is not covered in the above literature.

The current study is focused on developing and applying a systematic approach for exergy-and-cost flow-based analysis of STHXs. For this purpose, various design methods are critically examined for the thermal-hydraulic design of STHX. In addition, exergy analysis is conducted to calculate the flow exergy of all the streams as well as exergy destruction in the heat exchanger configuration. This is followed by an economic analysis that calculates various cost elements that applies to the current system. Also, the updated sensitivity of various influencing input parameters on the operational cost of HX is comprehensively investigated, in terms of normalized sensitivity coefficients. Finally, a cost optimum configuration is achieved by using the Genetic Algorithm.

To make the study useful for the readers, the manuscript is organized, systematically. In this regard, the first part is focused on the review of the economic optimization of STHX to identify the important parameters and their operating range. Section 2 covers the system description, governing equations, assumptions, and solution strategy. Thereafter in Section 3, the results and

discussion are presented. In Section 4 a general framework for the analysis of STHX as a preheater in a thermal desalination system is presented. Finally, the key findings are summarized in the last section.

Table 1.
Review of various studies on the economic optimization of STHXs using different algorithms.

Study	Method	Opt. Techniques	Objective	Constraints (min-max)	Outcome
Caputo et al. [28]	Kern	• Genetic Algorithm	• C_{total}	$D_{t,o}$: 0.01-0.051 m, D_s: 0.1-1.5 m L_{bc}: 0.05-0.5 m	↓C_{total} (≤ 50%)
Guo et al. [29,30]	Bell-Delaware	• EGM • Field Synergy • Genetic Algorithm	• S_{gen} • $\mathcal{E}$	$D_{t,o}$: ASTM values, B_c: 20-45% N_t: 50-500, L_{bc}/D_S: 201-100	↓C_{total} ↑$\mathcal{E}$
Ortega et al. [31]	Bell-Delaware	• Genetic Algorithm	• C_{total}	$D_{t,o}$: ASTM values, B_c:15-45%, N_P: 1-8, n_{pt}: 0-4, β: 30° and 90° Fluid side allocation	↓C_{total} (≤ 33%)
Patel and Rao [32]	Kern	• Particle Swarm Optimization	• C_{total}	$D_{t,o}$: 0.01-0.051 m, D_s: 0.1-1.5 m L_{bc}: 0.05-0.5 m, β: 30° and 90°	↓C_{total} (4-5%)
Sahin et al. [33]	Kern	• Artificial Bee Colony Algorithm	• C_{total}	N_t, $D_{t,o}$, L_t, L_{bc}, P_t	↓C_{total} (≤ 55%)
Hadidi et al. [34]	Bell-Delaware	• Imperialist competitive algorithm	• C_{total}	$D_{t,o}$: 0.01-0.051 m D_s: 0.1-1.5 m, L_{bc}: 0.05-0.5 m	↓C_{total} (≤ 53%)
Hadidi and Nazari [35]	Kern	• Biogeography-based algorithm	• C_{total}	N_t, D_s, $D_{t,o}$, L_t, L_{bc}, P_t	↓C_{total} (≤ 56%)
Asadi et al. [36]	Kern	• Cuckoo Search Algorithm.	• C_{total}	$D_{t,o}$: 0.008-0.051m, D_s: 0.2-0.9 m L_{bc}: 0.05-0.5 m	↓CAPC (≤ 13%) ↓OPC (≤ 77%)
Sadeghzadeh et al. [37]	Kern Bell-Delaware	• Genetic Algorithms • Particle Swarm Optimization	• C_{total}	$D_{t,o}$: 0.01-0.051 m, D_s: 0.1-1.5 m L_{bc}: 0.05-0.5 m	↓OPC (≤ 22%)
Khosravi et al. [38]	Bell-Delaware $\varepsilon - NTU$	• Genetic algorithm • Firefly algorithm • Cuckoo search algorithm	• $\mathcal{E}$ • C_{total}	N_t: 100-600, N_P: 1-3, L_t: 3-8, $D_{t,i}$: 0.0112-0.0172 m L_{bc}: 0.2-1.4, B_c: 0.19-0.32 (ratios) P_t / $D_{t,o}$: 1.25-3, β = 30°- 90°	↑$\mathcal{E}$ (≤ 83.8%)
Mohanty [39]	Kern	• Firefly Algorithm	• C_{total}	N_t, D_s, $D_{t,o}$, L_t, L_{bc}	↓C_{total} (≤ 29%)

Hajabdollahi et al. [40]	Bell-Delaware $\varepsilon-NTU$	• Genetic Algorithms • Sensitivity Analysis	• C_{total}	N_t: 100-600, N_P: 1-3, L_t: 3-8, $D_{t,i}$: 0.0112-0.0172 m, L_{bc}: 0.2-1.4, B_c: 0.19-0.32 (ratios) P_t / $D_{t,o}$: 1.25-3, β = 30°- 90° Fluid side allocation	↓C_{total} (≤ 35%)
Dhavle et al. [41]	Kern	• Cohort Intelligence Algorithm	• C_{total}	$D_{t,o}$: 0.01-0.051 m, N_P: 1-8, D_s: 0.1-1.5 m, L_{bc}: 0.05-0.5 m	↓C_{total} (≤ 52%)
Wen et al. [42]	Helical Baffle Correlations	• Genetic Algorithm (Kriging Metamodel)	• $\dot{Q}$ • C_{total}	Helical angles Baffle overlap ratio Inlet volume flow rate	↓C_{total} (≤ 32%)
Rao and Siraj [43]	Towler and Sinnott	• Elitist-Jaya Algorithm	• C_{total}	N_t, D_s, $D_{t,o}$, L_t, L_{bc}	↓C_{total} (≤ 33%)
Segundo et al. [44]	Kern	• Tsallis Differential Evolution	• C_{total}	D_s, $D_{t,o}$, L_{bc}	↓C_{total} (≤ 54%)
Tharakeshwar et al. [45]	Bell-Delaware	• Genetic Algorithm • Bat Algorithm	• ε • C_{total}	B_C, L_{bc}, P_t, L_t, β	↓C_{total} (≤ 14%)
Mirzaei et al. [46]	$\varepsilon-NTU$	• Constructal Theory • Genetic Algorithm	• ε • C_{total}	N_t, D_t, L_t	↑ε (28%) ↓C_{total} (≤ 32%)
Iyer et al. [47]	Kern	• Adaptive Range Genetic Algorithm	• C_{total}	$D_{t,o}$: 0.01-0.051 m, D_s: 0.1-1.5 m L_{bc}: 0.05-0.5 m, N_P: 1-8	↓C_{total} (≤ 52%)
Sai and Rao [48]	Kern	• Bacteria Foraging Algorithm	• ε • C_{total}	$D_{t,o}$, D_s, L_{bc}, N_P	↓C_{total} (≤ 2%)
Current study	Kern Bell-Delaware Wills Johnston	• Exergoeconomics • Normalized Sensitivity Analysis • Genetic Algorithm	• h/ΔP • NSC • X_D • C_{total}	Design parameters Operating parameters Fiscal parameters	↑Performance ↓X_D ↓C_{total}

↓: Decrease, ↑: Increase

2. System description and methodology

2.1. Heat exchanger configuration

The system considered in this study consists of a liquid-phase segmental-baffle STHX, which is used to preheat the water (in the tubes) by transferring heat from the hot stream on the shell-side, as shown in Figure 1. Two centrifugal pumps are used to maintain the required flow rate and pressure across the HX. The input data about the process parameters, i.e., fluid inlet-outlet temperatures and flow rates as well as the geometric parameters, are summarized in Table 2 [49].

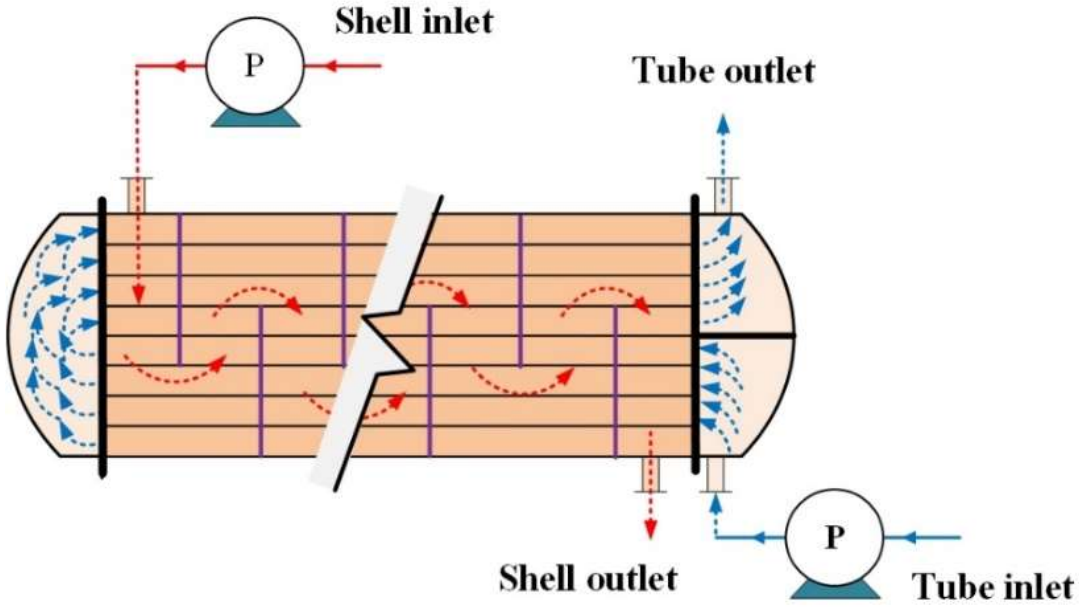

Figure 1. Schematic of heat exchanger configuration considered in the current study.

Table 2.
Specifications of the heat exchanger setup [49].

Parameter	Value
Process	
Mass flow rate (shell/tube), kg/s	27.80/68.90
Shell side temperature (inlet/outlet), °C	95/40
Tube side temperature (inlet/outlet), °C	25/40
Fouling resistance, R_f (shell/tube), m^2.K/W	0.00034/0.00020
Geometric	
Tube layout, *degree*	30°
Number of tube passes, N_p	2
Length of the tube, L_t, *m*	4.83
Tube internal diameter, $D_{t,i}$, *m*	0.016
Tube external diameter, $D_{t,o}$, *m*	0.020
Number of baffles, N_b	13
Baffle spacing, L_{bi}=L_{bo}=L_{bc}, *m*	0.356
Baffle cut, B_c, %	25
Number of pair of sealing strip, *Nss*	2
Diametral shell-to-baffle clearance, L_{sb}, *m*	0.0051
Diametral tube-to-baffle clearance, L_{tb}, *m*	0.0008
Baffle thickness, t_b, *m*	0.005
Tube pitch, L_{tp}, *m*	0.025
Bypass channel diametral gap, L_{bb}, *m*	0.019
Shell diameter, D_s, *m*	0.894
Number of the tube, N_t	918
Allowable operating pressure of tube side, P_t, *kPa*	100
Allowable operating pressure of shell side, P_s, *kPa*	100

112 *2.2. Thermal-hydraulic design*

113 This includes the calculation of tube and shell-side heat transfer coefficients (h_t *and* h_s),
114 pressure drops (ΔP_t and ΔP_s), overall heat transfer coefficient (U), and pumping power. For this
115 purpose, the Nusselt number (Nu) and friction factors (f) are calculated for both sides. The tube-
116 side calculations are straightforward; however, the shell-side calculations constitute a complex
117 mechanism because of several leakages, inaccuracies, and non-ideal flow streams, etc. Therefore,
118 the shell-side calculations for thermal-hydraulic performance are conducted using subsequent
119 approaches:

120 *2.2.1. Kern method*

121 Kern is the simplest method commonly used for the preliminary design of STHXs [4]. It is
122 based on the simplest case in STHX that neglects the presence of baffles. In this case, the flow is
123 across the tubes, and the heat transfer coefficient is similar to a concentric tube heat exchanger,
124 which could be calculated using equivalent diameter. Nevertheless, in actual practice, the baffles
125 significantly increase the h_s as well as ΔP_s due to turbulence. Moreover, the fluid velocity varies
126 because of the confined areas between the tubes across the tube bundle. Therefore, the correlations
127 for flow inside tubes are not appropriate for shell-side calculations. McAdams [50] proposed
128 formulation for the calculation of h_s as:

$$Nu = 0.36 Re^{0.55} Pr^{1/3} \phi^{0.14}$$
$$2\times10^3 < \mathrm{Re} < 1\times10^6, \quad \text{and} \quad Pr > 0.6 \tag{1}$$

129

130 The ΔP_s to fluid friction, apart from the nozzle losses, is estimated as [28].

$$\Delta P_s = \frac{\rho_s v_s}{2} f_s \frac{L_t}{L_{bc}} \frac{D_s}{D_e} \tag{2}$$

131

$$f_s = 2 b_o \mathrm{Re}_s^{-0.15} \tag{3}$$

132

133 where b_o is a constant, which is assumed to be, $b_o = 0.72$ by Peters and Timmerhaus [51]. This is
134 valid for Re < 40,000; however, the tube-side pressure drop can be estimated as [52]

$$\Delta P_t = \frac{\rho_t v_t^2}{2} \left(\frac{L_t}{D_{t,i}} f_t + p_c \right) N_p \tag{4}$$

135

$$f_t = \left(1.82 \log_{10} \mathrm{Re}_t - 1.64\right)^{-2} \tag{5}$$

136

The value of constant, p_c is also reported in the literature [49,52], which varies between 2.5 and 4 by these investigators.

2.2.2. Bell-Delaware method

It is the most accurate method for the design and analysis of STHXs as it acknowledges that there is only a portion of the fluid, which is over the tubes in a genuinely cross-flow arrangement [9]. The leftover fluid passes through the bypass areas because of the least resistance and constitutes up to 40% of the overall flow. Therefore, it is essential to consider the effects of non-ideal flow streams while performing thermal-hydraulic calculations [9]. For this purpose, the total flow is divided into several streams, i.e., tube hole leakage stream, cross-flow stream, the tube bundle bypass stream, the shell-to-baffle bypass stream, and the pass partition bypass stream. Therefore, h_s, is obtained as a product of the ideal cross-flow heat transfer coefficient, h_c, by the correction factors for the non-ideal cross-flow [9].

$$h_s = h_c J_C J_L J_B J_S J_R J_\mu \tag{6}$$

The ideal cross-flow heat-transfer coefficient (h_c) is calculated as [9],

$$h_c = j_i \, c_p G \, \mathrm{Pr}^{-2/3} \tag{7}$$

$$j_i = a_1 \left(\frac{1.33}{L_{tp} / D_t} \right)^a \mathrm{Re}^{a_2} \tag{8}$$

$$a = \frac{a_3}{1 + 0.14 \, \mathrm{Re}^{a_4}} \tag{9}$$

where Re is based on tube diameter. The significance and correlations for the calculation of correction factors (Js) in Eq. 6 as well as the values of a_1, a_2, a_3, and a_4 are given in Appendix A.

Similar to the heat transfer coefficient, the shell-side pressure drop is also calculated in three parts, i.e., the pressure drop in the central baffle spaces (ΔP_c), baffle windows (ΔP_w), entrance and exit baffle spaces (ΔP_e) [9].

$$\Delta P_f = \Delta P_c + \Delta P_w + \Delta P_e \tag{10}$$

These pressure drops are calculated using the correlation presented in Table 3.

Table 3.
Pressure drop correlations for the Bell-Delaware method [9].

Pressure drop	Governing equation
ΔP_c	$\Delta P_c = \Delta P_{bI}\left(N_b - 1\right) R_B R_L,\ \Delta P_{bI} = 0.002 f_I N_{tcc} \dfrac{G^2}{\rho} R_\mu$ $f_I = b_1 \left(\dfrac{1.33}{L_{tp}/D_t}\right)^b \mathrm{Re}^{b_2},\ b = \dfrac{b_3}{1+0.14\,\mathrm{Re}^{b_4}},\ R_B = \exp\left[-C_{bp} F_{sbp}\left(1-\sqrt[3]{2r_{ss}}\right)\right]$ $R_L = \exp\left[-1.33\left(1+r_s\right) r_{lm}^p\right],\ p = -0.15\left(1+r_s\right)+0.8,\ R_\mu = \left(\dfrac{\mu}{\mu_{wall}}\right)^{-m}$
ΔP_w	$\Delta P_{w,\mathrm{Turbulant}} = N_b \left[\left(2+0.6N_{tcw}\right)\dfrac{0.001 G_w^2}{2\rho}\right] R_L R_\mu$ $\Delta P_{w,\mathrm{Laminar}} = N_b \left\{26\left(\dfrac{G_w \mu}{\rho}\right)\left[\dfrac{N_{tcw}}{L_{tp}-D_t}+\dfrac{L_{bc}}{D_w^2}\right]+\left[\dfrac{0.002 G_w^2}{2\rho}\right]\right\} R_L R_\mu$ $G_w = \dfrac{\dot{m}}{\sqrt{S_m S_w}},\ D_w = \dfrac{4S_w}{\pi D_t N_{tw} + \left(\pi D_s \theta_{ds}/360\right)}$ $S_w = \dfrac{\pi D_s^2}{4}\left(\dfrac{\theta_{ds}}{360}-\dfrac{\sin\theta_{ds}}{2\pi}\right) - N_{tw}\left(\dfrac{\pi}{4}D_t^2\right)$
ΔP_e	$\Delta P_e = \Delta P_{bI}\left(1+\dfrac{N_{tcw}}{N_{tcc}}\right) R_B R_S,$ $R_s = \left(\dfrac{L_{bc}}{L_{bo}}\right)^{2-n} + \left(\dfrac{L_{bc}}{L_{bi}}\right)^{2-n}$

In the above equations ΔP_{bI}: ideal bundle pressure drop for one baffle compartment, f_I: friction factor, b_1-b_4: constants in Table A.1, R_B: bypass correction factor, R_L: leakage correction factor, $R\mu$: viscosity correction factor, D_w: hydraulic diameter, S_w: window area R_B: bypass correction factor,

2.2.3. Flow stream-analysis method

This method calculates the flow rates and pressure drops using a fundamental hydraulic model that was proposed by Wills-Johnston [4] as a simplified version of Palen and Taborek [53] work. For this purpose, the flow in the shell-side is divided into various streams as cross-flow, leakages, and bypass, as illustrated in Figure 2. The flow adopts different paths when moving from

A to B. These paths are specified by a subscript. For instance, the flow termed as “leakage” takes place between the tubes and baffles (t) and between the baffle and shell. Some of the flow passes over the tubes in a cross-flow (c), and part bypasses the tube bundle (b). The cross-flow and bypasses streams combine to form a combined window stream (w), which passes through the window zone. The shell side heat transfer coefficient is calculated using the actual cross-flow rate $\dot{m}_{cross}$ rather than the total shell-side flow rate, $\dot{m}_S$ as given in Eq. 11-13 [4].

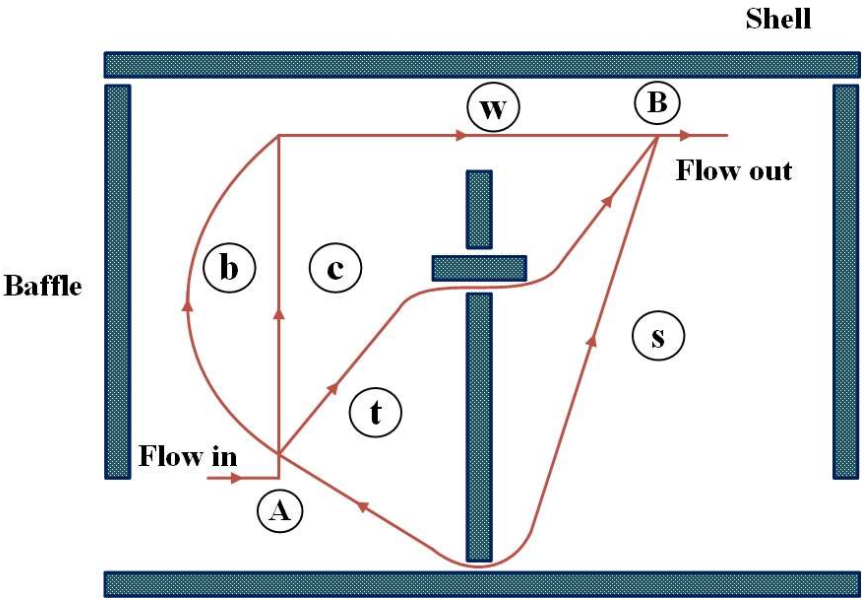

Figure 2. Equivalent shell-side flow [13].

$$Nu = 0.211 \mathrm{Re}^{0.651} \mathrm{Pr}^{0.34} \phi^{0.14} \tag{11}$$

$$\mathrm{Re} = \frac{\dot{m}_{cross} D_t}{\mu S_m} \tag{12}$$

where S_m is the cross-flow area, which is presented in Appendix A.

$$\dot{m}_{cross} = F_{cr} \dot{m}_S \tag{13}$$

Here F_{cr} is the portion of flow over the tube bundle in a cross-flow, which is calculated as.

$$F_{cr} = \frac{\left(\frac{n_p}{n_a}\right)^{0.5}}{\left(1 + \left(\frac{n_c}{n_b}\right)^{0.5}\right)} \tag{14}$$

For calculation of pressure drop, the ΔP between two points is taken the same irrespective of paths joining these points. The ΔP for all the streams is calculated in terms of the coefficient n_i and the respective mass flow rate $\dot{m}_i$ as

$$\Delta P_i = n_i \dot{m}_i^2 \tag{15}$$

The total shell side ΔP neglecting the inlet and exit nozzles are calculated as.

$$\Delta P = n_p \dot{m}^2 \left(N_b + 1 \right) \tag{16}$$

where, *n* represent the flow coefficients, which are constant, independent of flow rate, and is a function of geometry. The details regarding the calculation of flow coefficients are summarized in Appendix A.

2.3. Exergy analysis

Exergy is the maximum theoretical useful work that can be obtained from a system as it is brought into a complete thermodynamic equilibrium with the dead state [54]. The specific exergy of a fluid stream with negligible kinetic and potential energies is calculated as,

$$\overline{ex} = [(h' - h_0') - T_0(s - s_0)] + \overline{ex}_{che} \tag{17}$$

In the above equation $\overline{ex}_{che}$ represents the specific chemical exergy and has a non-zero value for streams with chemical potential such as brackish water, seawater, and brines [55–58].

The total exergy in "kW" of each stream is then calculated using the respective flow rate.

$$X = \dot{m}\overline{ex} \tag{18}$$

Finally, the exergy destruction in the pumps and heat exchanger is estimated by applying exergy balance equations. This gives,

$$X_{D,STHX} = X_{c,i} + X_{h,i} - X_{c,o} - X_{h,o} \tag{19}$$

$$X_{D,P} = X_{w,i} + \dot{W}_{P,i} - X_{w,o} \tag{20}$$

2.4. Economic analysis

This analysis involves the calculation of total cost (C_{total}) as a sum of capital cost (CAPC) and operating cost (OPC) i.e., $C_{total} = CAPC + OPC$. Conventionally, the CAPC is taken for heat exchangers only because of major share (compared to pumps) and the OPC is calculated using pumping power [28,37,47]. However, the current study covers exergoeconomic analysis as well, which calculates the stream cost using the costs of the heat exchanger as well as the pumps. The

details regarding the calculation of different steps involved in the economic analysis are discussed in the following sub-sections.

2.4.1. Capital cost

It reflects the component's purchasing cost and can be obtained through a market survey or supplier's quotations. However, the cost obtained by this method cannot accommodate design variations. It is, thus, limited for the specified case. Therefore, researchers have developed empirical correlations that can satisfactorily approximate the equipment cost based on the major design parameters like flow rates, heat transfer area, efficiency, pressure, and temperatures [59].

The capital cost of the centrifugal pumps in the current study is calculated using one of the most frequently reported correlations [60].

$$CAPC_{Pump} = 13.92\ \dot{m}_w \Delta P^{0.55} \left(\frac{\eta}{1-\eta} \right)^{1.05} \tag{21}$$

The calculation of the capital cost of STHX has been widely discussed because of its extensive use under different operating scenarios with varying thermal, hydraulic, and material bounds. In this reference, Shabani [61] proposed correlations that relate the capital cost with the weight of STHX as given in Eq. 22. Because the weight is not a true measure of heat exchange capacity, these correlations are rarely used in the literature.

$$CAPC = \exp\left[x_1 + x_2 \ln\left(W \right) \right] \tag{22}$$

where W is the weight in kg, and x_1 and x_2 are constants whose values are available in the literature [61].

Because of the heat transfer area (A) is an accurate indicator of STHX size and capacity, several correlations have been developed as a function of the area. In this regard, Turton et al. [62] provided a costing correlation for carbon steel (CS) STHX operating at ambient pressure of the form.

$$\log_{10} CAPC_{amb} = K_1 + K_2 \log_{10} A + K_3 (\log_{10} A)^2 \tag{23}$$

However, STHX with higher operating pressures and different construction materials, some additional constants and correction factors are multiplied with the base equation. This takes the form.

$$CAPC = CAPC_{amb} \left(B_1 + B_2 F_M F_P \right) \tag{24}$$

where F_M and F_P are the material and pressure correction factors, B_1 and B_2 are constants. These correlations have been used for the optimization of Organic Rankine Cycle STHX [25,63–65].

The most reliable and frequently used correlations for CAPC of STHX are those proposed by Hall et al. [66] and Taal et al. [67] using simple power law. The general form of these correlations is given as.

$$CAPC = x + yA^{Z} \tag{25}$$

where A is the heat transfer area in m^2 and x, y, z are constants which depend on the material of tubes and shell. Table 4 summarizes some of the useful correlations for CAPC of STHX.

Table 4.
Correlations for calculation of capital cost (*CAPC*) of the heat transfer equipment.

Correlation	**Material** (S/t)	**Ref.**
$CAPC^{\$} = 30800 + 750A^{0.81}$	CS-CS	[66]
$CAPC^{\$} = 30800 + 1339A^{0.81}$	CS-SS	[66]
$CAPC^{\$} = 30800 + 1644A^{0.81}$	SS-SS	[66]
$CAPC^{\$} = 7000 + 360A^{0.8}$	CS-CS	[67]
$CAPC^{\$} = 1000 + 324A^{0.91}$	SS-SS	[67]
$CAPC^{\$} = 8500 + 409A^{0.85}$	CS-SS	[38,40,42,45,46,67,68]
$CAPC^{€} = 8000 + 259.2A^{0.91}$ (✓)	SS-SS	[19,28,30,32–37,39,43,44,47,67,69]
$CAPC^{\$} = 10205 + 11.52A$	CS-CS, A (ft^2)	[70]
$\log_{10} CAPC^{\$} = K_1 + K_2 \log_{10} A + K_3 (\log_{10} A)^2$	CS-CS	[25,63–65]
$CAPC^{\$} = 3.28 \times 10^4 \left(A/80\right)^{0.68}$		[71,72]

(✓) currently used

Caputo et al. [73] critically reviewed these correlations, given all the processes involved in STHX manufacturing. They highlighted several limitations of these correlations and proposed a very rigorous approach to calculate the STHX cost. The approach involves the calculation of material cost as well as the cost of all manufacturing processes like drilling, cutting, beveling, chamfering, and welding, which is used to manufacture shells, tube sheets, tube bundles, baffles, channels, and flanges, individually. It is comparatively more reliable and flexible for STHX optimization, particularly from the manufacturing perspective. However, for performance analysis of STHX as a system component, this detailed approach is not computationally economical.

Hence, the purchased equipment cost correlations based on the heat transfer area rather than manufacturing cost reasonably serve the purpose.

Moreover, it is essential to emphasize that the correlations discussed above and used in the current study were developed about 30 years back. The cost calculated using these correlations is precise only for the time they were developed [73]. Therefore, it is appropriate to improve these correlations to recent times using cost indices to accommodate the inflation and variations in the market scenarios [25]. For this purpose, the idea of using a cost index factor (C_{index}) has been adopted [24,65]. The C_{index} is calculated using the Chemical Engineering Plant Cost Index (CEPCI) of the reference year and the current year [63].

$$C_{index} = \frac{CEPCI_{current}}{CEPCI_{reference}} \tag{26}$$

Thus, the current CAPC of the equipment is given as [64],

$$CAPC^{\$}_{current} = C_{index} \times CAPC^{\$}_{reference} \tag{27}$$

In the present study, the C_{index} is calculated to be 1.7 based on the $CEPCI_{1990}$ = 390 [74] and $CEPCI_{2020}$ = 650 [75]. However, for rigorous design and analysis purposes, the effect of C_{index} is also studied in this paper for a wide range of values.

2.4.2. Operational cost

The OPC is calculated based on current annual cost C_o (\$/y), equipment life, n_y (year), unit electricity price, C_{elec} (*\$/kWh*), annual inflation rate, i (%), operational availability Λ (*hour*), and pumping power, PP, (*kW*) as.

$$OPC = \sum_{j=1}^{n_y} \frac{C_o}{(1+i)^j} \tag{28}$$

$$C_o = PP \times C_{elec} \times \Lambda \tag{29}$$

$$PP = \left(\frac{\dot{m}_{tube}\ \Delta p_{tube}}{\rho_{tube}} + \frac{\dot{m}_{Shell}\ \Delta p_{Shell}}{\rho_{Shell}} \right) \times \frac{1}{\eta} \tag{30}$$

In the current case study, the values of fiscal parameters are taken as n_y = 10 year, = 7000 *h/y*, i = 10%, C_{elec} = 0.12 (*\$/kWh*) and $\eta = 70\%$ [28].

2.4.3. Exergoeconomic analysis

After the calculation of capital and operational cost, the analysis is applied to calculate the stream cost [76]. For this purpose, the CAPC calculated above is first converted to the annual rate of capital investment $\dot{Z}\,(\$/y)$ using the capital recovery factor (CRF) [77]. The CRF is calculated based on the interest rate (i) and amortization years/economic life of the plant (n_y), as given below [78]:

$$CRF = \frac{i \times (1+i)^{n_y}}{(1+i)^{n_y} - 1} \tag{31}$$

$$\dot{Z} = CRF \times CAPC \tag{32}$$

Finally, the rate of fixed cost ζ (in \$/s) is calculated using the plant availability (Λ) as [79].

$$\zeta = \frac{\dot{Z}}{3600 \times \Lambda} \tag{33}$$

After that, a general cost balance equation is applied to each component in the system. This is expressed as [80].

$$\dot{C}_o = \Sigma \dot{C}_i + \zeta \tag{34}$$

where $\dot{C}_o$ represents the local output stream cost, $\dot{C}_i$ the cost of the input stream, and ζ the rate of fixed (purchased equipment) cost.

The cost balance equation for the pump and heat exchanger, respectively, are given as:

$$\dot{C}_o = \dot{C}_i + C_{elec}\dot{W}_{Pump} + \zeta_{Pump} \tag{35}$$

$$\dot{C}_{c,o} = \dot{C}_{c,i} + \dot{C}_{h,i} - \dot{C}_{h,o} + \zeta_{STHX} \tag{36}$$

It is important to mention that for the components with multiple outlet streams (i.e., heat exchangers, evaporators, flash chambers and membrane modules, etc.), additional auxiliary equations are required. For a system with "k" outlet streams, "k-1" number of auxiliary equations are required to solve the system [21]. These equations are based on the equality of the inlet and outlet streams cost averaged with exergy of the respective streams as given in Eq. 37 [81].

$$\frac{\dot{C}_{h,i}}{X_{h,i}} - \frac{\dot{C}_{h,o}}{X_{h,o}} = 0 \tag{37}$$

311 *2.5. Sensitivity analysis*

312 Sensitivity analysis is an important tool to ascertain insight into the significance of model
313 parameters and, in turn, identify those, which are more responsive [82]. The results of this analysis
314 not only help in improving the system performance but also highlight the important areas for future
315 research [83]. Calculus-based sensitivity analysis is one of the most fundamental and reliable
316 methods for this purpose. This method models each independent parameter as a sum of its nominal
317 value and the perturbation or uncertainty as given below [84].

318 $$X = \bar{X} \pm \hat{U}_X \tag{38}$$

319 where $\bar{X}$ is the nominal value and $\pm\hat{U}_X$ is possible uncertainty about the nominal value. The
320 corresponding uncertainty in the response variable $Y(X)$ due to uncertainty in X is expressed in a
321 differential form as [85],

322 $$\hat{U}_Y = \frac{dY}{dX}\hat{U}_X \tag{39}$$

323 For a multi-variable function $Y = Y(X_j, X_{j+1}, \ldots, X_N)$, the uncertainty in Y due to the
324 perturbations in the X is calculated as the root sum square product of the individual perturbation
325 computed to the first-order accuracy, as given in Eq. 40. Each partial derivative in the equation
326 represents the sensitivity coefficient (SC), which depicts the sensitivity of output parameters to
327 small changes in the respective input parameter [86].

328 $$\hat{U}_Y = \left[\sum_{j=1}^{N}\left(\frac{\partial Y}{\partial X_j}\hat{U}_{Xj}\right)^2\right]^{1/2} \tag{40}$$

329 Meanwhile, a more convenient and comprehensive way of presenting the findings of sensitivity
330 analysis is through Normalized Sensitivity Coefficients (NSC) [87]. It allows the direct (one-on-
331 one) comparison of parameters whose order of magnitude could be significantly different [88].
332 These NSCs are obtained by normalizing the uncertainties in the response parameter Y and input
333 parameter X by its respective nominal values. For this, the coefficients in Eq. 40 are transformed
334 into NSC and normalized uncertainties (NU) as given by [89].

335 $$\frac{\hat{U}_Y}{\bar{Y}} = \left[\sum_{j=1}^{N}\overbrace{\left(\frac{\partial Y}{\partial X_j}\frac{\bar{X}_j}{\bar{Y}}\right)^2}^{NSC}\overbrace{\left(\frac{\hat{U}_{Xj}}{\bar{X}_j}\right)^2}^{N\bar{U}_{Xj}}\right]^{1/2} \tag{41}$$

In the current study, the sensitivity of input parameters like mass flow rate, inlet-outlet temperatures, baffle spacing, and fiscal parameters (interest rate and electricity cost) on the output parameters i.e., h, ΔP, OPC, and $C_{S,o}$ is studied. The equations developed and used for this analysis are given as follows.

$$\frac{\hat{U}_{h_S}}{\overline{h}_S}=\left[\begin{array}{l}\left(\frac{\partial h_S}{\partial \dot{m}_S}\frac{\overline{\dot{m}}_S}{\overline{h}_S}\right)^2\left(\frac{\hat{U}_{\dot{m}_S}}{\overline{\dot{m}}_S}\right)^2+\left(\frac{\partial h_S}{\partial L_{bc}}\frac{\overline{L}_{bc}}{\overline{h}_S}\right)^2\left(\frac{\hat{U}_{L_{bc}}}{\overline{L}_{bc}}\right)^2+\left(\frac{\partial h_S}{\partial T_{S,i}}\frac{\overline{T}_{S,i}}{\overline{h}_S}\right)^2\left(\frac{\hat{U}_{T_{S,i}}}{\overline{T}_{S,i}}\right)^2\\+\left(\frac{\partial h_S}{\partial T_{S,\mathrm{o}}}\frac{\overline{T}_{S,\mathrm{o}}}{\overline{h}_S}\right)^2\left(\frac{\hat{U}_{T_{S,o}}}{\overline{T}_{S,\mathrm{o}}}\right)^2\end{array}\right]^{1/2} \tag{42}$$

$$\frac{\hat{U}_{\Delta P_S}}{\overline{\Delta P_S}}=\left[\left(\frac{\partial\overline{\Delta P_S}}{\partial \dot{m}_S}\frac{\overline{\dot{m}}_S}{\overline{\Delta P_S}}\right)^2\left(\frac{\hat{U}_{\dot{m}_S}}{\overline{\dot{m}}_S}\right)^2+\left(\frac{\partial\overline{\Delta P_S}}{\partial L_{bc}}\frac{\overline{L}_{bc}}{\overline{\Delta P_S}}\right)^2\left(\frac{\hat{U}_{L_{bc}}}{\overline{L}_{bc}}\right)^2\right]^{1/2} \tag{43}$$

$$\frac{\hat{U}_{OPC}}{\overline{OPC}}=\left[\begin{array}{l}\left(\frac{\partial\overline{OPC}}{\partial \dot{m}_S}\frac{\overline{\dot{m}}_S}{\overline{OPC}}\right)^2\left(\frac{\hat{U}_{\dot{m}_S}}{\overline{\dot{m}}_S}\right)^2+\left(\frac{\partial\overline{OPC}}{\partial L_{bc}}\frac{\overline{L}_{bc}}{\overline{OPC}}\right)^2\left(\frac{\hat{U}_{L_{bc}}}{\overline{L}_{bc}}\right)^2+\left(\frac{\partial\overline{OPC}}{\partial C_{elec}}\frac{\overline{C}_{elec}}{\overline{OPC}}\right)^2\left(\frac{\hat{U}_{C_{elec}}}{\overline{C}_{elec}}\right)^2\\+\left(\frac{\partial\overline{OPC}}{\partial i}\frac{\overline{i}}{\overline{OPC}}\right)^2\left(\frac{\hat{U}_i}{\overline{i}}\right)^2\end{array}\right]^{1/2} \tag{44}$$

$$\frac{\hat{U}_{C_{S,o}}}{\overline{C}_{S,o}}=\left[\begin{array}{l}\left(\frac{\partial C_{S,o}}{\partial \dot{m}_S}\frac{\overline{\dot{m}}_S}{\overline{C}_{S,o}}\right)^2\left(\frac{\hat{U}_{\dot{m}_S}}{\overline{\dot{m}}_S}\right)^2+\left(\frac{\partial C_{S,o}}{\partial L_{bc}}\frac{\overline{L}_{bc}}{\overline{C}_{S,o}}\right)^2\left(\frac{\hat{U}_{L_{bc}}}{\overline{L}_{bc}}\right)^2+\left(\frac{\partial C_{S,o}}{\partial C_{elec}}\frac{\overline{C}_{elec}}{\overline{C}_{S,o}}\right)^2\left(\frac{\hat{U}_{C_{elec}}}{\overline{C}_{elec}}\right)^2\\+\left(\frac{\partial C_{S,o}}{\partial i}\frac{\overline{i}}{\overline{C}_{S,o}}\right)^2\left(\frac{\hat{U}_i}{\overline{i}}\right)^2\end{array}\right]^{1/2} \tag{45}$$

Finally, the relative contribution (RC) of each parameter is estimated to identify the dominant uncertainty contributors by combining the sensitivity coefficients with the actual uncertainty [88]. Its mathematical form is obtained as the square of the product of sensitivity coefficient and uncertainty, normalized by the square of the uncertainty in the response parameter [89].

$$RC=\frac{\left(\frac{\partial Y}{\partial X_j}\hat{U}_{Xj}\right)^2}{\hat{U}_Y^2} \tag{46}$$

2.6. Numerical solution and assumptions

The mathematical model discussed above is solved using an Engineering Equation Solver (EES) based numerical code. In the first step, the input data consisting of flow rates, temperatures, and geometric parameters are provided. The EES library routines are used to calculate the thermophysical properties and correction factors for STHX. After that, the code works using algorithms of the three methods (i.e., Kern, Bell-Delaware, and Wills-Johnston). For the Kern method, the Nu and ΔP are calculated directly using Eq. 1, 2, and 4 which also involve the calculation of Re, friction factor, equivalent diameter, etc.

While, the Bell Delaware method additionally focuses on the calculation of ideal heat transfer coefficient (given in Eq. 7), ideal pressure drop for baffle compartment, window cross areas, window tubes. Besides, the method also involves the calculation of correction factors (presented in Table A.2) i.e., baffle cut, baffle leakage, bundle bypass, un-equal baffle spacing, laminar flow, and wall viscosity correction factor, etc. These correction factors are used in Eq. 6 and to calculate the shell side heat transfer coefficient. Similarly, in this method, the total shell side pressure drop is calculated in three portions i.e., across the tube bundle, in the window zone, and inlet and exit baffles. These individual pressure drops add up to the total pressure drop given in Eq 10.

In the Wills-Johnston method, the parameters like flow fractions and resistances i.e., combined flow, cross flow, bypass flow, shell side flow, tube side flow, window flow, and end window flow resistance are determined first using relations presented in Table A.3. Thereafter these are used to calculate the crossflow rate, Re, Nu, shell side local/overall heat transfer coefficient, and total shell side pressure drop using Eqs. (11) – (16). The total shell side pressure drop is the sum of the pressure drop at the central window and the pressure drop at the end window zones.

In each case, the numerical code is validated with the literature for all three methods followed by a comprehensive thermal, hydraulic, exergetic, and exergoeconomic analysis of STHX, as summarized in Fig. 3. Finally, the genetic algorithm is employed to optimize the heat exchanger design taking cost as an objective function (for which the working is discussed in detail in subsequent Section 4.5). The analysis is based on the following assumptions: (a) steady-state operation, (b) negligible longitudinal conduction, (c) uniform heat transfer coefficients, (d) negligible heat and pressure losses in the connecting pipes, and (e) no thermal energy source or sink in the HX or fluid.

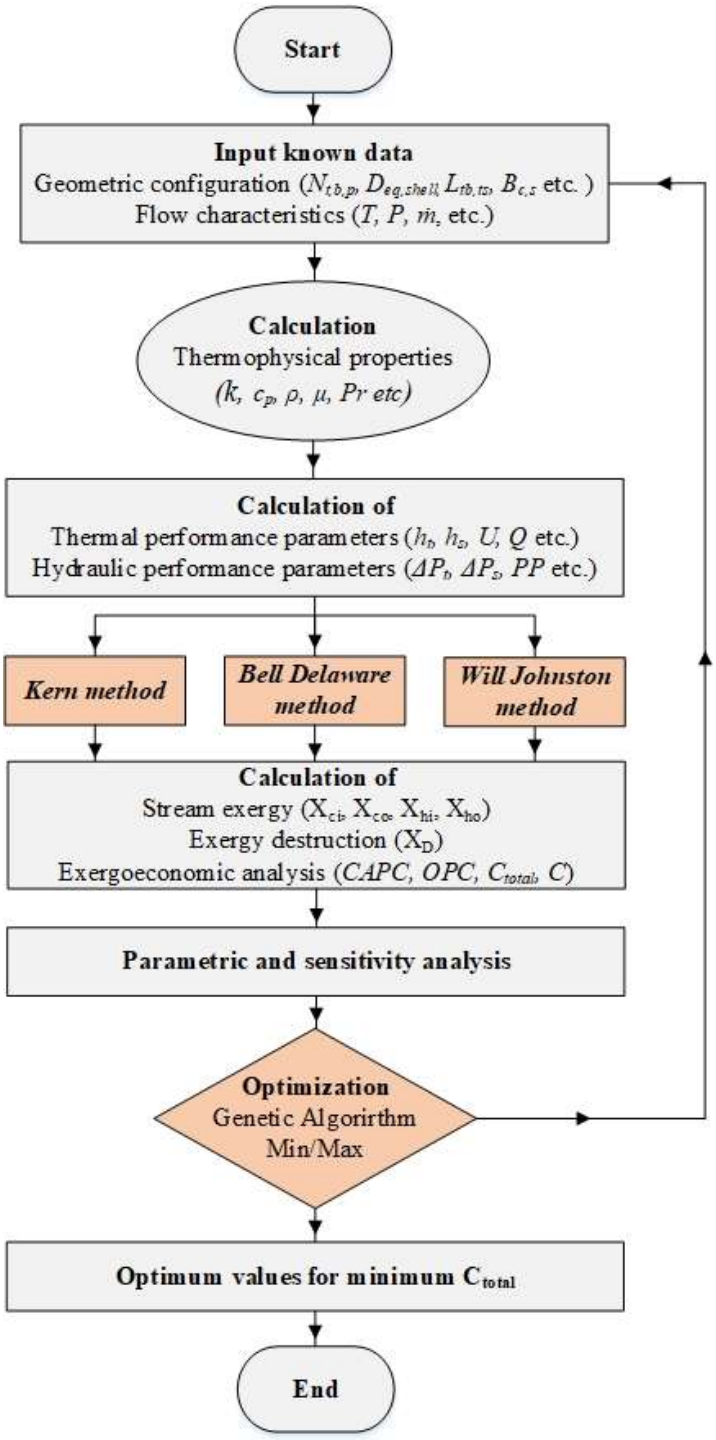

Figure 3. Solution flow chart.

3. Results and discussion

3.1. Numerical model validation

The EES-based numerical code was developed to solve the governing equations of Kern, Bell-Delaware, and Wills-Johnston's methods, in addition to validation with the literature, as presented in Table 5. The first two methods are validated with the case discussed by Sinnott and Towler [49], which is recently used by Caputo et al. [28] and Sadeghzadeh et al. [37]. The case is based on a methanol-to-brackish water heat exchanger with a triangular pitch and a heat duty of 4.34 MW with one shell and two-tube-side passes. The inlet and out temperatures and flow rates are as follows $T_{S,i} = 95^{\circ}C$, $T_{t,i} = 25^{\circ}C$, $T_{S,o} = 40^{\circ}C$, $T_{t,o} = 40^{\circ}C$, $\dot{m}_S = 27.80$ kg/s, and $\dot{m}_t = 68.90$ kg/s. While the third method (i.e., Wills-Johnston) is validated with the case presented by Serth [90]. It involves kerosene-to- crude oil heat exchanger with a heat duty of 1.089 MW, one shell- and four tube-side passes. The process parameters used are $T_{S,i} = 390^{\circ}F$, $T_{t,i} = 100^{\circ}F$, $T_{S,o} = 250^{\circ}F$, $T_{t,o} = 150^{\circ}F$, $\dot{m}_S = 45000$ lb/h, and $\dot{m}_t = 150{,}000$ lb/h.

The results showed a reasonable agreement between the values obtained by the current analysis and literature values. However, a remarkable deviation (±12 %) is observed in the shell-side heat transfer coefficient calculated by using the Kern method. This is presumably because of the empirical heat transfer correlation that does not consider various leakages and baffle configurations in the Kern method, while the other two methods consider all the possible effects in developing the heat transfer and pressure drop correlations. It is important to note that the remaining results are satisfactorily close to the values reported in the literature for all the cases.

404 **Table 5.**

405 Validation of Kern and Bell Delaware and Wills Johnston methods numerical code.

Parameters	**Values**		
	Literature [28,37,49]	**Present work**	**Error %**
A, m^2	278.6	278.6	0 %
$Q\ (MJ)$	4.34	4.34	0 %
S_s, m^2	0.06365	0.06365	0%
$h_t, W/m^2k$	3812	3811	± 0.026 %
$\Delta P_t, Pa$	6251	6166	± 1.35 %
$C_{total}, €$	64,480	64,266	± 0.331 %
Kern method			
Re	18,381	18,572	± 1.039 %
$h_s, W/m^2k$	1573	1791*	± 12.171 %
$\Delta P_s, Pa$	35,789	35,166	± 1.740 %
Bell-Delaware method			
Re	26,353	24,176	± 8.260 %
$h_s\ W/m^2k$	1246	1159	± 6.982 %
$\Delta P_s\ Pa$	8050	8054	± 0.049 %
Wills-Johnston method [90]			
S_b, ft^2	0.03583	0.03583	± 0 %
F_{cr}	0.345	0.345	± 0 %
Re	10,569	10,531	± 0.359 %
$h_s, btu/h.\ ft^2F$	----	177.6	----
$\Delta P_s, psi$	1.25	1.27	± 1.6 %

406 *: major difference, ----: Not available

407

3.2. Heat exchanger design

The above validated numerical code is employed to design a liquid-phase water-water STHX using Kern, Bell-Delaware, and Wills-Johnston methods. The process and geometric parameters used as input data are summarized in Table 2. The output parameters, including heat transfer coefficients, pressure drops, pumping power, exergy destruction, capital, operational, and stream costs, are calculated and presented in Table 6. It also presents a rationale comparison of two commonly used (i.e., Kern and Bell-Delaware) and one rarely adopted (i.e., Wills-Johnston) STHX design methods from thermal, hydraulic, exergetic, and economic viewpoints. It is observed that; the Kern method shows a significant over/underestimation of shell-side parameters compared to Bell-Delaware (which is known to be the most accurate STHX design method). For instance, the shell-side heat transfer coefficient, pressure drop, pumping power, operational and total costs calculated using the Kern method deviates from those calculated using Bell-Delaware by ±56%, ±330%, ±100%, ±100%, and ±4.85%, respectively; however, for Wills-Johnston, these deviations are significantly lower with ±7.4%, ±49%, ±15%, ±15%, and ±0.8%, respectively.

It is important to mention that the large-scale deviations in the Kern method are primarily because it ignores the effect of baffles and associated leakages on the shell-side flow. While the other two methods accommodate the presence of baffles through correction factors and flow coefficients. Therefore, it is reasonable to assert that the reliability of the design and analysis of STHX conducted is the highest for Bell-Delaware followed by Wills-Johnston and then Kern method. Particularly, from a monetary viewpoint, the Kern method is only suitable for preliminary sizing, however, for a satisfactory design, the other two methods should be preferred to reduce capital and operation investments associated with the over and underestimations.

Table 6.

A preliminary design with three methods i.e., Kern, Bell-Delaware, and Wills-Johnston.

Parameter	Case study: Water to Water STHX		
	Kern	Bell-Delaware	Wills-Johnston
A, m^2	■ 278.6	278.6	278.6 ■
Re_t	■ 15,779	15,779	15,779 ■
$h_t, W/m^2K$	■ 4053	4053	4053 ■
Re_s	▼ 15,095	19,621	4281* ▼
$h_s, W/m^2K$	▲ 4300	2748	2952 ▲
$U, W/m^2K$	▲ 854	768	785 ▲
$\Delta P_t, Pa$	■ 6098	6098	6098 ■
$\Delta P_s, Pa$	▲ 27,786	6447	3257 ▼
$h_s/\Delta P_s, m/s\ K$	▼ 0.1548	0.4262	0.9065 ▲
PP, kW	▲ 1.73	0.8648	0.7354 ▼
$X_{D\ Total}, kW$	▲ 685	684	684 ▼
$CAPC_{HX}, €$	■ 87,562	87,562	87,562 ■
$CAPCt_{otal}, €$	▲ 89,589	88,936	88,751 ▼
$\dot{Z}_{total}, €/h$	▲ 2.083	2.068	2.064 ▼
$OPC, €$	▲ 8931	4464	3796 ▼
$C_{total}, €$	▲ 96,492	92,025	91,357 ▼
$\dot{C}_{c,o}, €/h$	▲ 2.282	2.169	2.151 ▼
$\dot{C}_{h,o}, €/h$	▲ 0.00845	0.00227	0.00126 ▼

▲: Overestimation, ▼: Underestimation, ■: Same

* The major difference is because of cross-flow which is merely 0.3 to 0.5 of the total flow

3.3. Sensitivity analysis

The sensitivity analysis outcomes in the form of Normalized Sensitivity Coefficients (NSC) and Relative Contribution (RC) for the Bell-Delaware method are summarized in Figure 4 (a) to (d). The results are presented for critical input parameters (for which NSC ≥ 0.0001). Figure 4 (a) highlights the input parameters that have an impact on the shell-side heat transfer coefficient. It shows that for the given case, the most critical parameters in terms of NSC are shell-side flow rate $\dot{m}_S$, followed by shell inlet temperature $T_{S,i}$, central baffle spacing L_{bc}, and shell outlet temperature $T_{S,o}$, respectively. While, the RC is dominated by the uncertainty in $\dot{m}_S$ with 98% followed by L_{bc} $T_{S,i}$, and $T_{S,o}$, with 2%, 0.11%, and 0.10%, respectively.

Similarly, Figure 4 (b) shows that the shell-side pressure drop (ΔP_S) is the most sensitive to the L_{bc} followed by $\dot{m}_S$. However, the relative contribution is higher ~76% for $\dot{m}_S$ and lower for L_{bc} with ~23% and almost insignificant for inlet and outlet temperatures. The operational cost displays (refer Figure 4 (c)) the highest NSC for unit electricity cost (C_{elec}) with ~1, followed by $\dot{m}_S$ with ~0.78, L_{bc} with ~0.4, and interest rate (i) with ~0.2, respectively. The corresponding RC values are 65%, 20%, 9%, and 3%, respectively. Concurrently, the stream cost shows (see Figure 4 (d)) the highest NSC for $\dot{m}_S$, followed by L_{bc}, C_{elec}, and i, respectively. The RC values are calculated as ~ 86% for $\dot{m}_S$, ~11% for L_{bc}, ~1.8% for C_{elec}, and ~0.05% for i.

The findings of the sensitivity analysis infer that the thermal-hydraulic performance (i.e., h and ΔP) of STHXs is sensitive to the flow characteristics, and the economic performance is equally governed by the fiscal parameters such as unit electricity cost and interest rate. Therefore, a commensurate importance should be apportioned to the fiscal parameters while conducting the economic analysis of heat exchangers. It is also important to emphasize that the discrepancies between maximum NSC and RC values for dissimilar parameters are well explained by James et al. [88]. This is because the small uncertainties associated with the highest sensitivity coefficients shift the relative contribution toward the input parameters with lower-sensitivity coefficients, especially those with high uncertainties. Moreover, it is also worth mentioning that one order of magnitude alteration (as adopted in the sensitivity analysis) is usually not of practical interest, rather it should be perceived only as a limiting case to obtain directly comparable values.

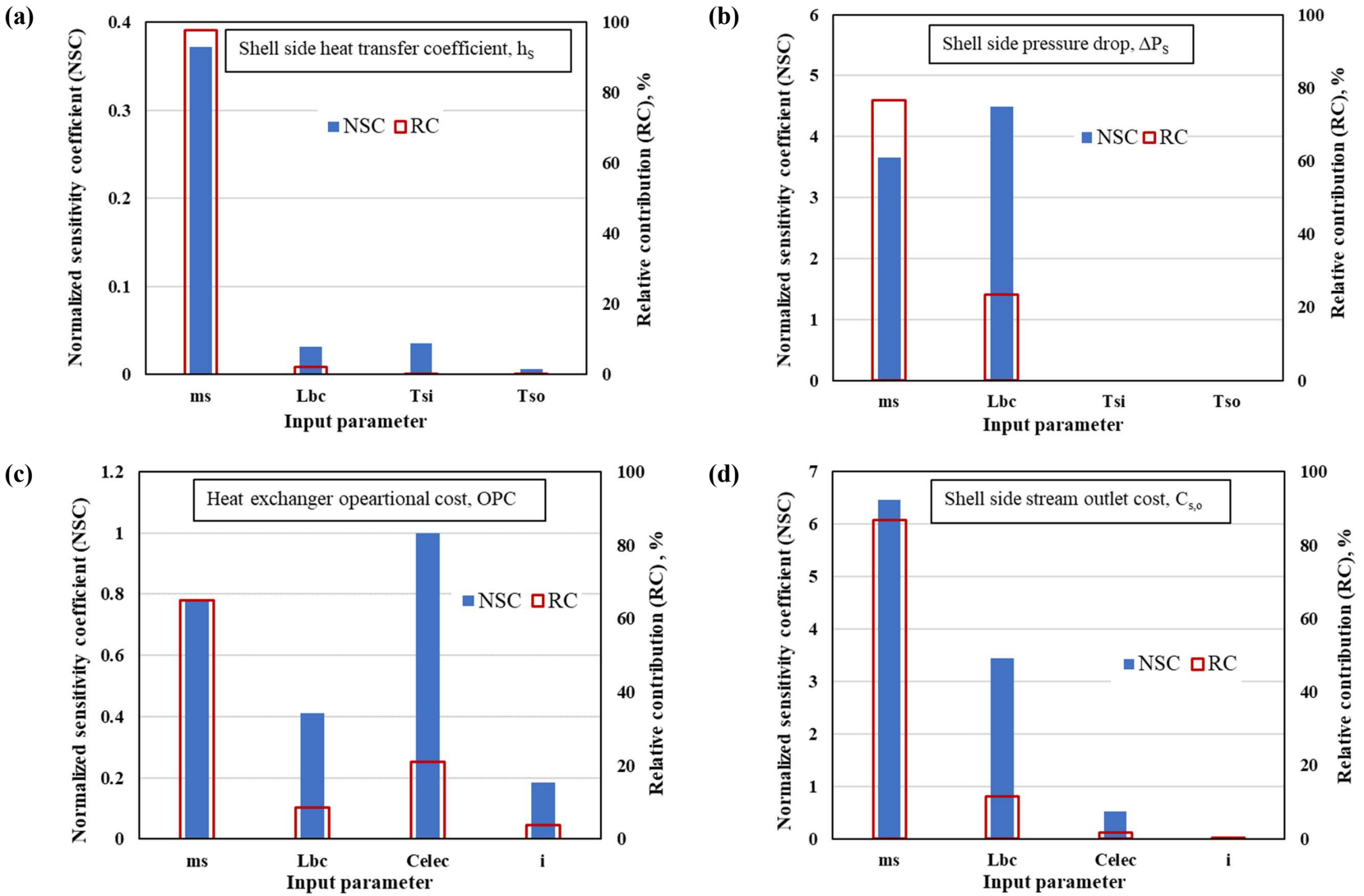

Figure 4. Sensitivity analysis results, i.e., NSC and RC of different input parameters on performance parameters (a) h_S, (b) ΔP_S, (c) OPC, and (d) $C_{o,s}$.

3.4. Parametric analysis

A detailed parametric analysis is conducted using the one-factor-at-a-time (OFAT) approach to investigate the real scale effect of important input parameters on the thermal, hydraulic, and economic performance of STHX. The results are presented combinedly for Kern, Bell-Delaware, and Wills-Johnston methods, which illustrate the deviation of three methods (from each other) over a range of operating conditions.

3.4.1. Effect of shell-side flow rate

The mass flow rate is one of the most influential process parameters (as indicated by the sensitivity analysis) that governs the thermal, hydraulic, and economic performance of heat exchangers. It is observed that an increase in shell-side flow-rate increased the heat transfer coefficient (h_s); however, the corresponding pressure drop (ΔP) also increased as shown in Figure 5 (a) and (b). This is because the higher flow rate resulted in a higher shell-side Reynolds number, which intensified the turbulence that controls the heat transfer rate and pressure drops. Hence, there should be a tradeoff between the heat transfer coefficient and pressure drop for optimal performance. In this regard, the heat transfer coefficient per unit pressure drop ($h/\Delta P$) gives a reasonable estimation of the overall thermal-hydraulic performance of heat exchangers. From Figure 5 (c), it is seen that an increase in shell-side flow rate decreased the $h/\Delta P$ showing a higher-order rise in the pressure drop compared to the heat transfer capability. However, up to 15-20 kg/s, the $h/\Delta P$ is well above unity showing higher heat transfer than pressure drops.

Similarly, an increase in the shell-side flow rate increased the operating and stream (product) cost as shown in Figure 6. For instance, the operational cost calculated using Bell-Delaware and Wills-Johnston methods varied from ~3,000 to 10,000 € for flow rate varying from 1 to 50 kg/s. While for the Kern method, it approached ~34,000 € for the same flow rate variations, which indicate the overestimation of hydraulic and economic parameters and the limitations of the Kern method at higher flow rates. Likewise, the cold water outlet stream cost approached 2.3 €/h for Bell-Delaware and Wills-Johnston methods, while above 2.8 €/h for the Kern method. A similar trend is observed for the hot water outlet stream with different magnitudes (varying between 0.005 to 0.01 €/h for Bell-Delaware and Wills-Johnston methods, and 0.040 €/h for the Kern method. From these observations, it is reasonable to assert that the Kern method gives a very rough estimate regarding the heat exchanger design, particularly at high flow rates. Hence, for a practical design, the other two methods should be preferred to minimize energy and monetary investments.

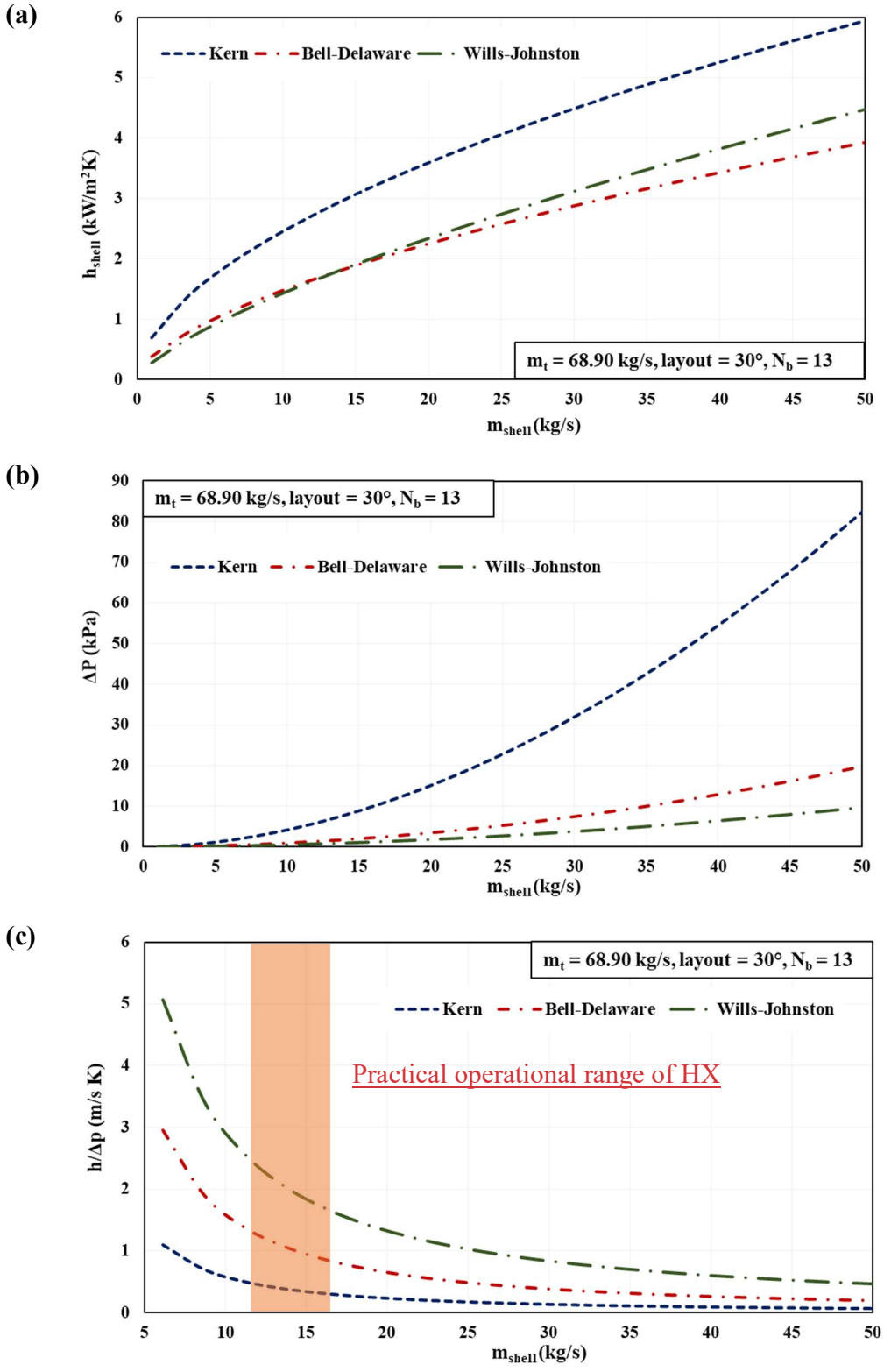

Figure 5. Effect of shell-side flow rate on (a) heat transfer coefficient, (b) pressure drop, and (c) h/ΔP

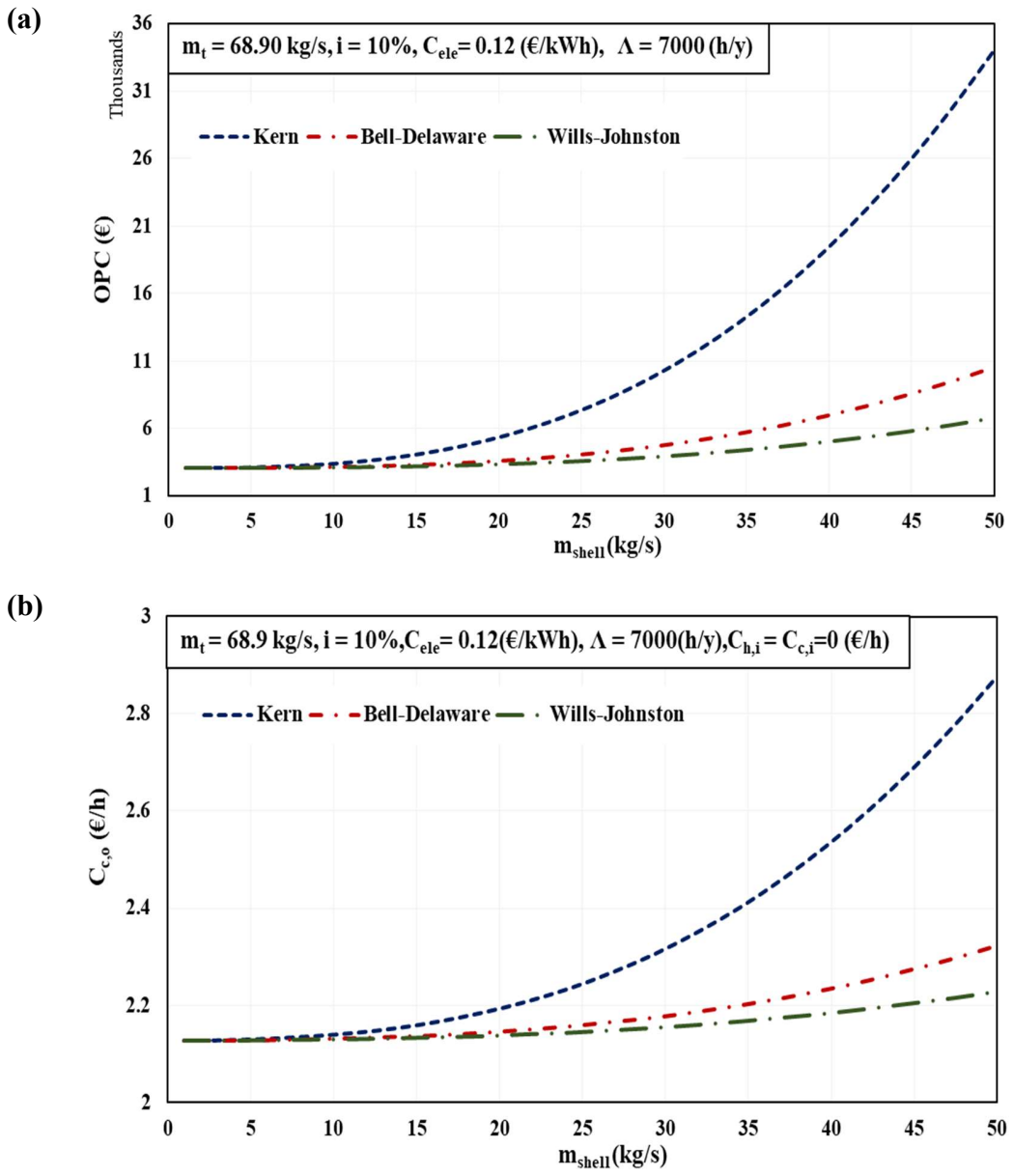

Figure 6. Effect of shell-side flow rate on (a) operational cost, and (b) cold water outlet stream cost.

3.4.2. Effect of number of baffles

One of the objectives of baffles is to support the tube bundle against weight, high flow rates, and pressures to mitigate the vibrations. However, their presence also influences the shell-side thermal-hydraulic performance by obstructing the flow, as illustrated above by normalized sensitivity coefficients. Figure 7 (a) and (b) show that an increase in the number of baffles (N_b) increased the shell-side heat transfer coefficient as well as pressure drops. For example, h_s increased to 3 kW/m^{2}K for Bell-Delaware and Wills-Johnston methods and ~5 kW/m^{2}K for the Kern method from 1.82 kW/m^{2}K for N_b varying from 2 to 15. The corresponding variations in pressure drops are calculated as 5 kPa and 8 kPa for Bell-Delaware and Wills-Johnston and 50 kPa for the Kern method. While, the h/ΔP factor decreased with an increase in N_b, thus showing a higher-level rise in the pressure drop than the heat transfer coefficient (refer Figure 7 (c)).

Besides, from a monetary viewpoint, it is noticed that (refer to Figure 8 (a)) the operational cost of STHX increased with increasing N_b due to higher pressure drop and pumping power. For instance, an increase in N_b from 2 to 15, increased the operational cost from 3,200 € to 4,900 € for Bell-Delaware and up to 4,100 € Wills-Johnston methods. While the corresponding cost for the Kern method is 14,000 €. Similarly, the cold water outlet stream cost showed a ~2.34% increase for Bell-Delaware and Wills-Johnston methods and ~12% for the Kern method. A similar trend is also observed for the other outlet stream cost with different magnitudes. It is also noticed that the diversions in thermal, hydraulic, and economic parameters calculated using Bell-Delaware and Wills-Johnston methods from the Kern method become more significant at higher N_b values. This is primarily because of the effect of not reliable pressure drop calculations of the Kern method, which amplified at a higher number of baffles.

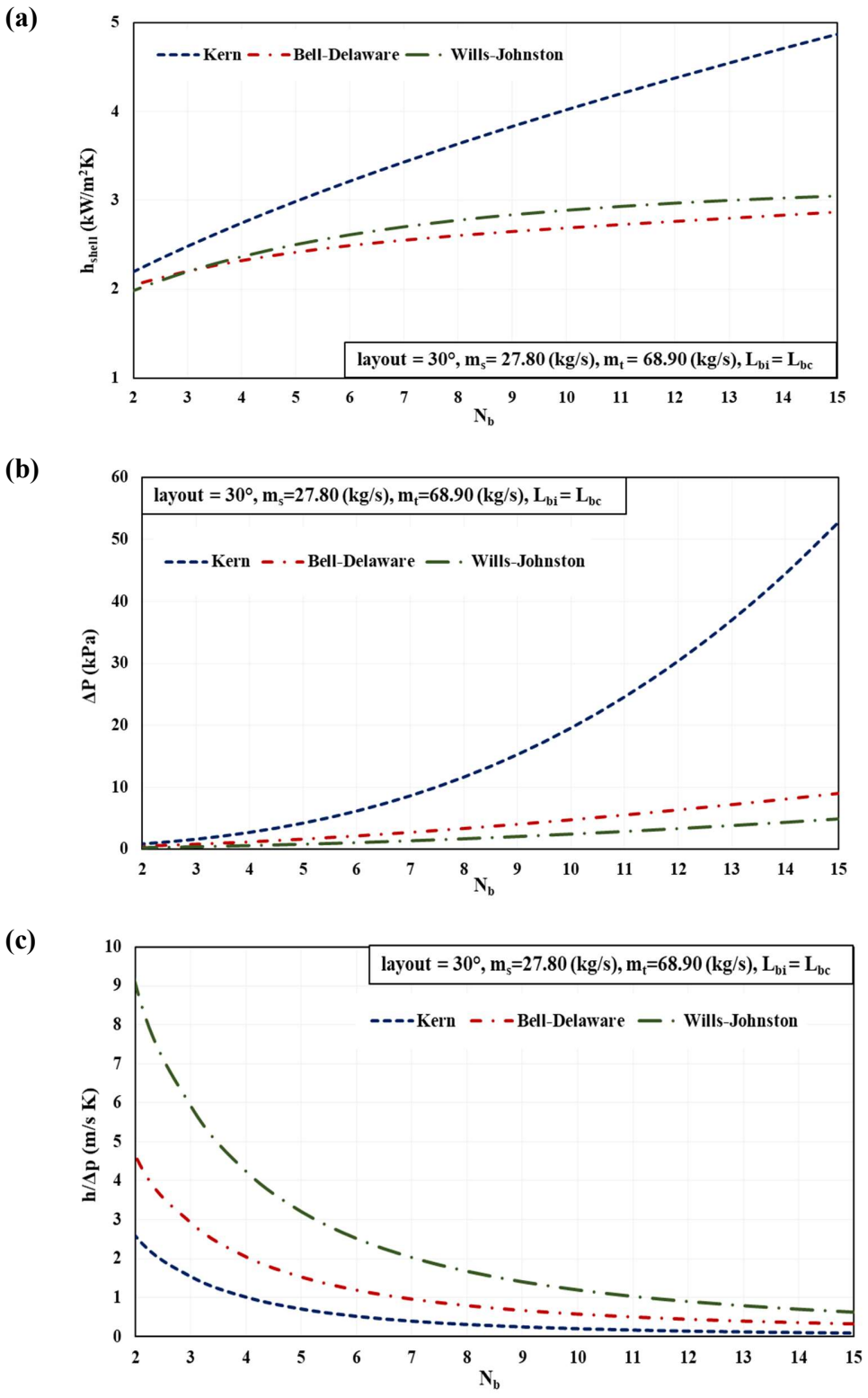

Figure 7. Effect of number of baffles on (a) shell side heat transfer coefficient (b) pressure drop, and (c) h/ΔP

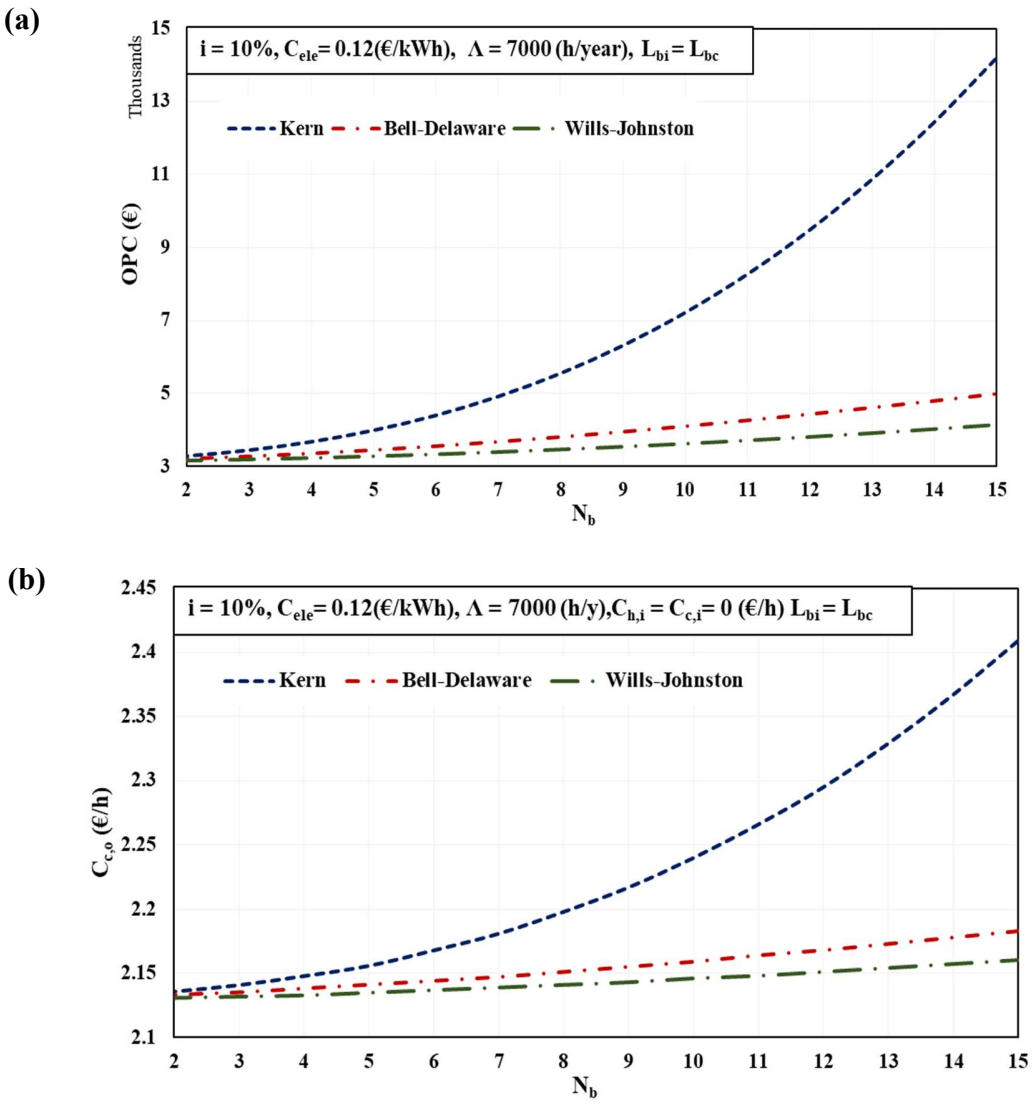

Figure 8. Effect of the number of baffles on (a) operational cost and (b) cold water outlet stream cost.

3.4.3. Effect of fiscal parameters

The conventional studies on heat exchangers are mainly focused on investigating the effects of process and design parameters on the thermodynamic and economic performance. However, analysis of the combined effect of fiscal and process parameters has gained significant attention for a rigorous thermoeconomic analysis of systems [24,26]. This is because, the systems with the same thermodynamic performance, operating in different regions and/or times with dissimilar economic policy (interest rate, energy price, chemical cost, etc.) will have substantially different operational costs [76,77]. Moreover, the sensitivity analysis also expressed a significant influence of fiscal parameters on the economic performance of STHXs in the above sections. Therefore, this investigation can satisfactorily predict an overall heat exchanger performance for the assorted operating scenarios.

In this regard, Figure 9 (a) and (b) illustrate the effect of the cost index factor (C_{index}) on the total-and-stream costs. The figure shows a linear rise in the total cost (C_{total}) and stream outlet cost over the years. For example, C_{total} of the heat exchanger configuration increased by ~70% from ~55,000 € to ~93,000 € over 30 years because of market inflation. Consequently, the stream cost surged to 2.3 €/h from 1.3 €/h during this period. A similar variation in the product cost is observed with the interest rate, as shown in Figure 9 (c). It is seen that a heat exchanger (with the same thermal-hydraulic performance) operating in two different regions with dissimilar interest rates will have significantly different product costs. For instance, the product cost of cold water outlet stream showed an increase of ~30% (from 1.6 to 2.1 €/h) for an STHX operating at interest rates of 4% and 10%, respectively.

Similarly, the product cost of an STHX operating at different unit electricity costs is shown in Figure 9 (d). It shows the significance of pressure drop, particularly for situations with high unit energy prices. Moreover, significant deviation in the OPC calculated using the Kern method from Bell-Delaware and Wills-Johnston method (which grow with increasing C_{elec}) indicate rough pressure drop calculations. Besides, the chemical cost can also be an influential parameter for HXs subjected to high fouling tendency fluids. However, an accurate antifoulant cost estimation requires dynamic modeling of fouling propensity.

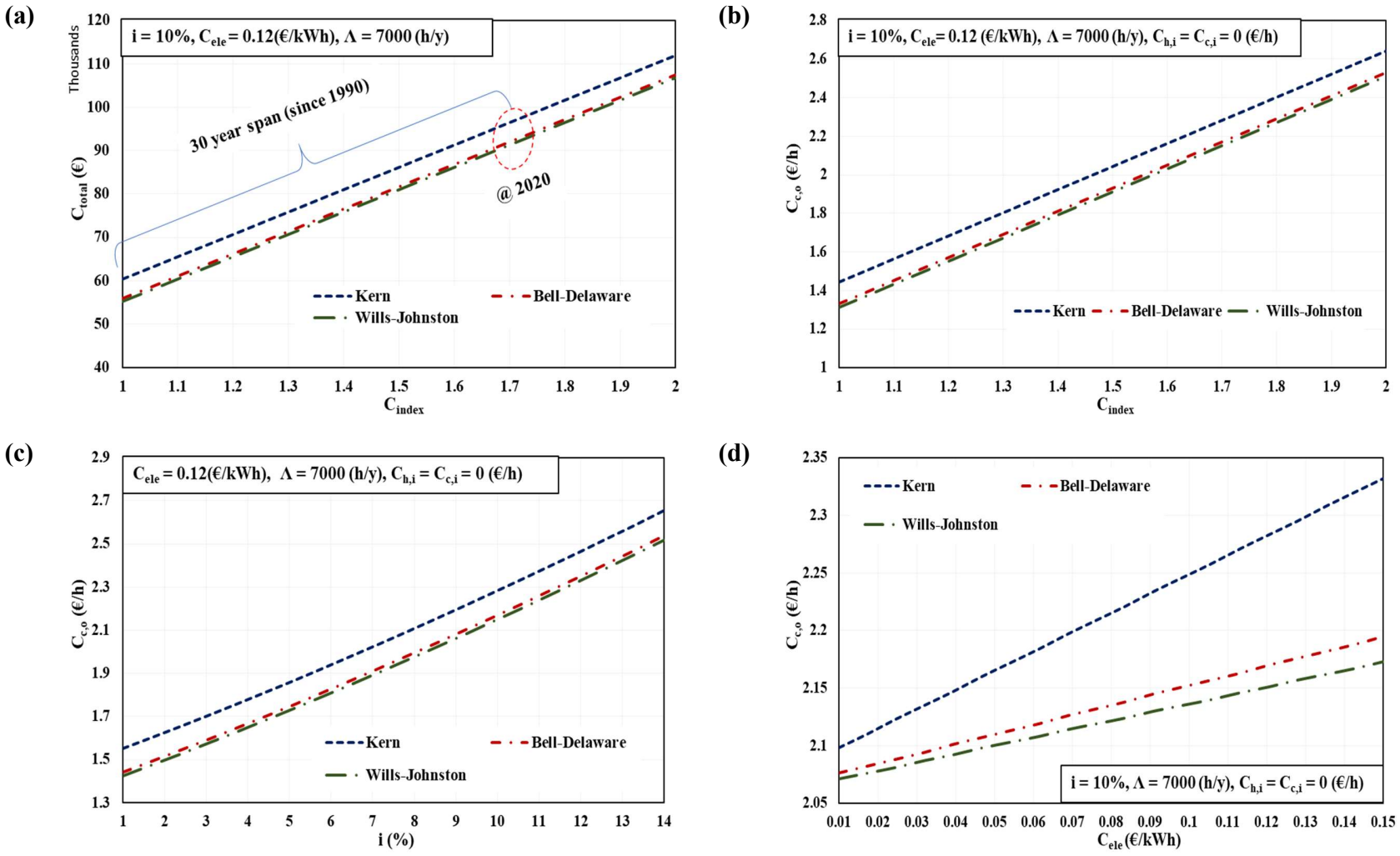

Figure 9. Effect of fiscal parameters (a) total cost versus cost index factor, (b) cold water outlet cost versus cost index factor, (c) cold water outlet cost versus interest rate, and (d) cold water outlet cost versus unit electricity cost.

3.4.4. *Exergy-and-cost flow diagram*

The exergy-and-cost flow diagram is an important pictorial illustration of thermodynamic and monetary performance at each unique point of the system. It presents the cost (exergy and economic) of all streams in the system at inlets and outlets of the components calculated using fixed and recurring expenses. This diagram is particularly important for the systems with a large number of components (e.g., power plants, desalination systems, etc.) compared to simple heat exchangers. This is because it indicates exergy (in kW) and cost rates (in €/time), which are reliable indicators of how efficiently the energy and economic resources are continuously utilized by each component rather than merely relying on the investments at the system boundaries. The exergy-and-cost flow diagram for the heat exchanger configuration considered in this study is presented in Figure 10.

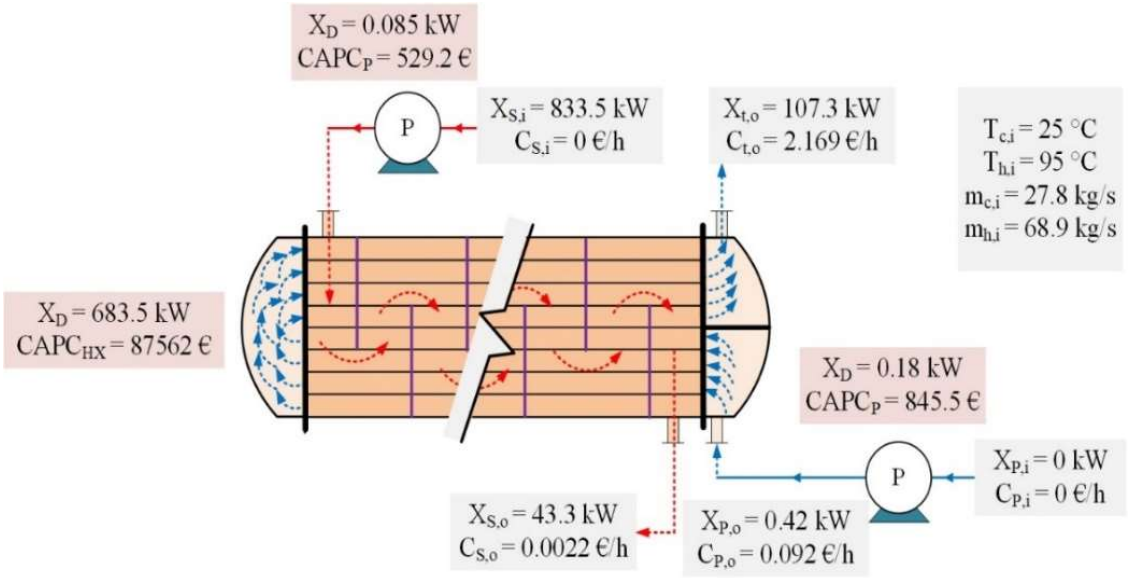

Figure 10. Exergy-and-cost flow diagram of the heat exchanger arrangement.

3.5. *Optimization*

After a detailed design sensitivity and parametric analyses, the optimization of STHX is conducted using the Genetic Algorithm (GA). The GA is a biological evolution based natural algorithm in which the survival gene (best individual point) replaces the old gene to get the optimum solution. The objective function (fitness) is defined first, which allows each potential solution to be evaluated. Then the estimated range of design variables and termination criteria is

582 selected, and a random initial population is developed in the range of design variables. After the
583 initialization of the population, the algorithm sets the arrangement of the new population (next
584 generation) repeatedly and perform the iterations until the termination criterion is met. Each point
585 (gene) contains a solution that is evaluated with the parent solution based on the fitness. If the gene
586 fulfills the criteria it replaces the parent solution and becomes a new parent (current best solution).
587 Otherwise, the algorithm selects the pervious optimum parents and produce children (next
588 generation or genes) by mutation or crossover of parent's and replace the population with children
589 to produce the next generation. The process is continued until the criteria are attained. The
590 termination criteria refer to either the best-optimized solution or the maximum number of
591 generations. The algorithm picks the best individual point with better-optimized results as a parent
592 and eliminates the inferior solution. This framework will guarantee that the algorithm converges
593 to the best individual point which will be the best-optimized solution for the selected objective
594 function [29,31,37]. The solution flowchart for GA is presented in Figure 11.
595 In the current study, the minimum total cost C_{total} is used as an objective function against seven
596 constraint variables, including tube layout, tube outside diameter, number of tubes, tube passes,
597 shell diameter, baffle cut, and baffle spacing. The upper and lower bounds for these constraints are
598 selected carefully from the literature [28,31,38,40], as summarized in Table 7. The values of
599 algorithm-specific parameters i.e., generations = 100, population size = 100, and mutation
600 probability = 0.035 are taken as reported by Sadeghzadeh et al. [37].

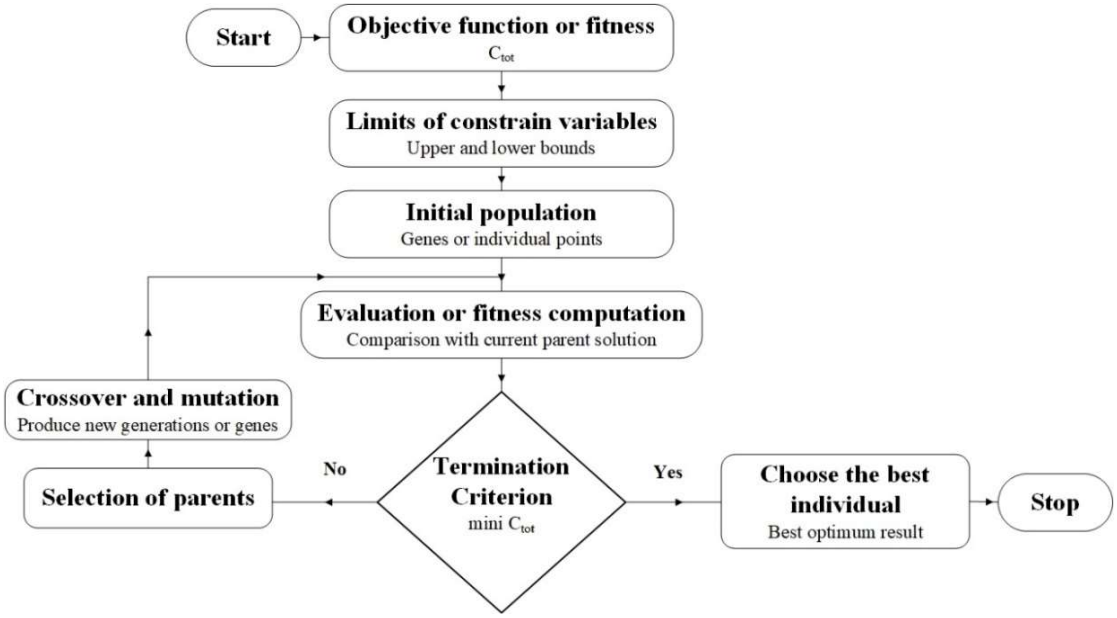

601
602 **Figure 11.** Flow chart of GA.

Table 7.

The lower, upper, and optimum value of the design variable for STHX [28,31,38,40].

Parameters	Constraint bounds		
	Lower	Upper	Optimum*
Layout	30°	90°	30°
Shell diameter, m	0.1	1.5	1.483
Tube outside diameter, m	0.015	0.051	0.01501
Baffle cut ratio, B_c	0.20	0.35	0.3141
Baffle spacing, m	0.05	0.5	0.489
Number of tube passes	1	8	1
Number of tubes	900	2000	901

***** calculated,

Note: Not all references provided all data ranges.

The optimization is performed for all three methods (i.e., Kern, Bell-Delaware, and Wills-Johnston), and the values for standard and optimal STHX are presented in Table 8. Owing to the highest reliability, the discussions are made concerning the Bell-Delaware method in detail. It is observed that the optimization altered the STHX performance, significantly, as indicated by various thermal, hydraulic, and economic parameters. For example, the tube side heat transfer coefficient and the shell side heat transfer coefficient decreased by ~2.2% and ~21.7%, respectively, which decreased the overall heat transfer coefficient by ~7.7%. Meanwhile, the corresponding tube- and shell-side pressure drops reduced much more significantly (than heat transfer coefficients) by ~43.8% and ~66.6%, respectively, thus decreasing the pumping power by ~50.7%.

Accordingly, the comprehensive thermal-hydraulic performance indicator (i.e., $h/\Delta P$) increased by ~2.3 folds, indicating improved thermodynamic performance. Meanwhile, because of modifications in design parameters, the number of tubes decreased slightly, but the shell diameter increased. The optimal heat transfer area was reduced by ~26.4%, resulting in a ~20.5% cut in the capital cost. Similarly, the operational cost observed a ~50.7% reduction because of pumping power. Finally, the total cost decreased by ~22%, which reduced the cold water production (stream) cost from 2.16 to 1.68 €/h (~21%). A similar trend can also be observed for the other two methods with somewhat different magnitudes.

Overall, it is summarized that the sensitivity analysis and optimization of conventional STHX appreciably improved the design and analysis process. Therefore, the modern thermal system studies should be extended to normalized sensitivity analysis and optimization through any of the numerical techniques (Genetic Algorithm, Particle Swarm Optimization, etc.) rather than simply relying on conventional parametric analysis.

Table 8.
Parameters of optimal shell-and-tube heat exchanger using a genetic algorithm.

Parameter	Kern		Bell-Delaware		Wills-Johnston	
	Standard	**Optimal**	**Standard**	**Optimal**	**Standard**	**Optimal**
Re_t	15,779	10,727	15,779	10,727	15,779	10,727
h_t, W/m^2K	4053	3964	4053	3964 ↓	4053	3964
Re_s	15,095	4974	19,651	6608	4281	2299
h_s, W/m^2K	4300	3110	2748	2150 ↓	2952	2623
U, W/m^2K	854	789	768	709 ↓	785	756.3
ΔP_t, Pa	6098	3426	6098	3426 ↓	6098	3426
ΔP_s, Pa	27,786	10,168	6447	2150 ↓	3257	1090
$h_s/\Delta P_s$, $m/s\ K$	0.1548	0.305	0.4262	1 ↑	0.9065	2.407
PP, kW	1.73	0.75	0.8648	0.426 ↓	0.7354	0.383
$X_{D\ total}$, kW	685	684	684	684	684	684
A, m^2	278.6	205	278.6	205 ↓	278.6	205
$CAPC_{HX}$, €	87,562	69,582	87,562	69,582 ↓	87,562	69,582
$CAPCt_{otal}$, €	89,589	70,878	88,936	70,478 ↓	88,751	70,397
$\dot{Z}_{total}$, €/h	2.083	1.648	2.068	1.639 ↓	2.064	1.637
OPC, €	8931	3878	4464	2200 ↓	3796	1978
C_{total}, €	96,492	73,460	92,025	71,782 ↓	91,357	71,560
$\dot{C}_{c,o}$, €	2.282	1.735	2.169	1.689 ↓	2.151	1.682

↓: Decrease, ↑: Increase

4. Analysis of STHX as a preheater in a desalination system

Preheaters are used in thermal desalination systems to recover heat from brine and distillate streams, respectively as a brine and distillate preheaters. The recuperated energy is used to preheat the intake seawater which improves the system performance from an energy, exergy, economic, and environmental viewpoint. The schematic diagram for a conventional desalination system with STHX as an energy recovery section is shown in Figure 12. Meanwhile, it is also important to note that for more narrow temperature control and ease of maintenance, the plate and frame heat exchangers are also preferred [91]. A comprehensive theoretical framework for a component-based exergoeconomic analysis and optimization of the whole plant is presented in Eq. 47-57 [92].

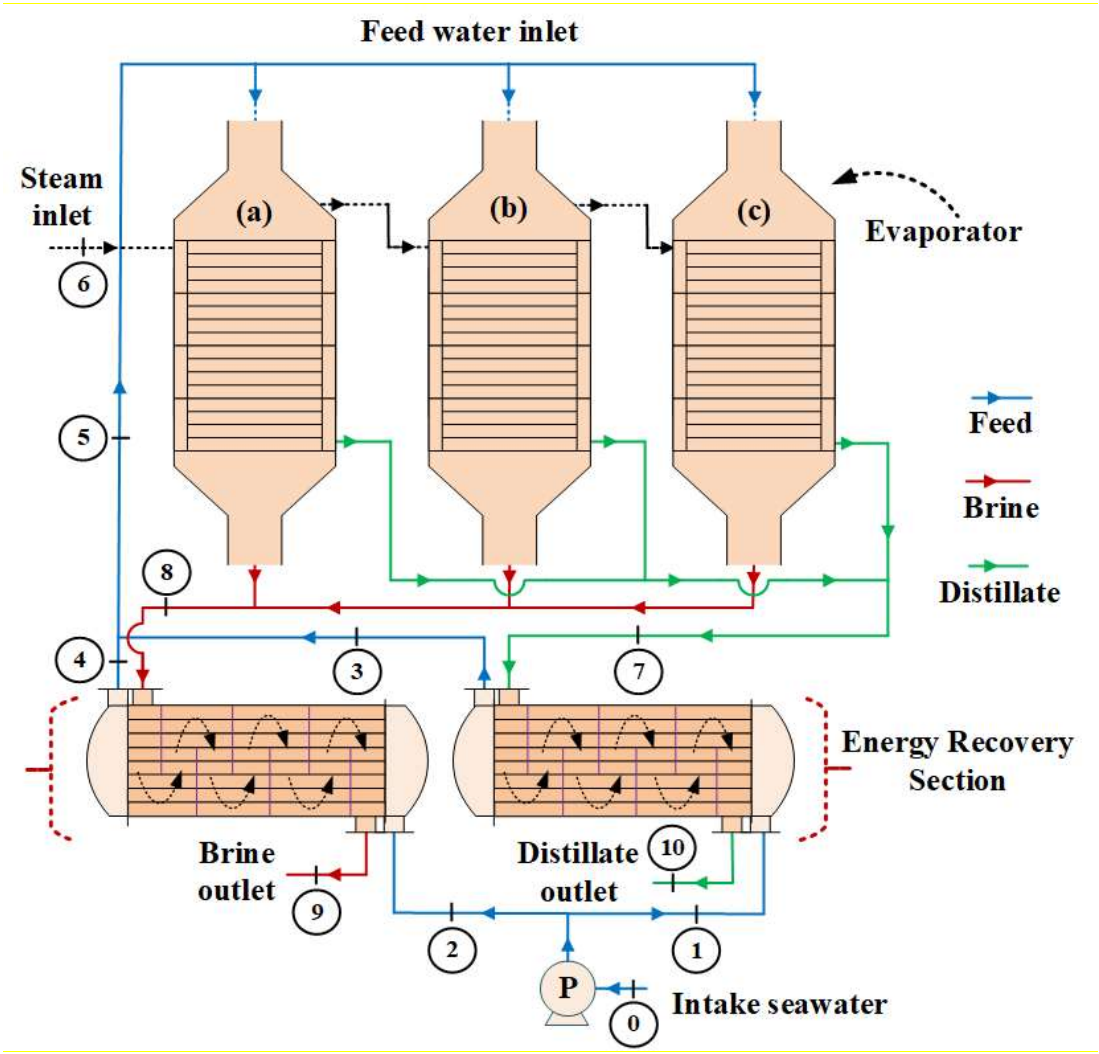

Figure 12. Thermal desalination system with STHX as an energy recovery section.

644 The cost at the pump outlet is calculated using the capital cost of pump, electricity consumption,
645 and unit electricity cost as:

646 $$\dot{C}_1 = \psi\left(\dot{C}_0 + C_{elec}\dot{W}_{Pump} + \zeta_{Pump}\right) \quad (47)$$

647 $$\dot{C}_2 = (1-\psi)\left(\dot{C}_0 + C_{elec}\dot{W}_{Pump} + \zeta_{Pump}\right) \quad (48)$$

648 where ψ is the feed split ratio between the two preheaters (e.g., ψ = 0.5 indicates an equal
649 distribution of feed in both the preheaters.

650 The feed water cost at distillate preheater and brine preheater outlet is calculated using the
651 capital cost of the respective preheater (i.e., STHX) and auxiliary equation as:

652 $$\dot{C}_3 = \dot{C}_1 + \dot{C}_7 - \dot{C}_{10} + \zeta_{DH} \quad (49)$$

653 $$\frac{\dot{C}_1}{X_1} = \frac{\dot{C}_3}{X_3} \quad (50)$$

654 $$\dot{C}_4 = \dot{C}_8 + \dot{C}_2 - \dot{C}_9 + \zeta_{BH} \quad (51)$$

655 $$\frac{\dot{C}_8}{X_8} = \frac{\dot{C}_9}{X_9} \quad (52)$$

656 The overall feed cost at the evaporator inlet is taken as a sum of the streams from both the
657 preheaters, as

658 $$\dot{C}_5 = \dot{C}_3 + \dot{C}_4 \quad (53)$$

659

660 The distillate cost at the evaporator outlet is calculated using inlet steam cost, feed cost, and
661 capital cost of the evaporation section. Two auxiliary equations required to solve the evaporator
662 section are also given below.

663 $$\dot{C}_7 = \dot{C}_5 + \dot{C}_6 - \dot{C}_8 + \zeta_{Evaporator} \quad (54)$$

664 $$\frac{\dot{C}_5}{X_5} = \frac{\dot{C}_8}{X_8} \quad (55)$$

665 $$\frac{\dot{C}_6}{X_6} = \frac{\dot{C}_7}{X_7} \quad (56)$$

666 Finally, the water production cost is calculated using the overall distillate cost and the water
667 production capacity of the plant.

$$\dot{C}_{fw}(\$ / \mathrm{m}^3) = \frac{\dot{C}_9 + \dot{C}_{10} + \dot{C}_{misc}}{\dot{V}_D} \quad (57)$$

where, $\dot{C}_{misc}$ is the miscellaneous cost such as blowdown, cooling, condensate, chemical, post-treatment, etc.

5. Concluding remarks

A liquid-phase segmental baffle shell-and-tube heat exchanger was investigated from thermal, hydraulic, exergy, and economic viewpoint. Three design approaches, i.e., Kern, Bell-Delaware, and Wills-Johnston (flow stream) were used for thermal-hydraulic modeling. An exergy-and-cost flow-based analysis procedure was presented to calculate fluid stream costs. A normalized sensitivity analysis is carried out to identify the most influential input parameters in the form of normalized sensitivity coefficients and relative contributions. Then a detailed parametric analysis was conducted to investigate the real scale effect of input parameters using the one-factor-at-a-time approach. Finally, the design was optimized for the minimum total cost by employing the Genetic Algorithm. Under the operating conditions considered in this study, some significant findings were drawn as follows.

- The flow-stream analysis method of Wills-Johnston, though used rarely, can predict shell-side thermal-hydraulic parameters reasonably close to the Bell-Delaware method (±10%).
- Kern method is only useful for approximate preliminary sizing of STHX because of large scale over/underestimation (> ±100%) of heat transfer coefficient and pressure drops which govern the heat exchanger cost.
- The deviation of the Kern method intensified (±200%) at a higher number of baffles and flow rates because of the augmented effects of baffles, which are not accounted for precisely in the Kern method.
- The sensitivity analysis showed that thermal performance (h_S) of STHX is sensitive to the input parameters in the following order with normalized sensitivity coefficient (NSC) magnitudes as, $\dot{m}_S$ (NSC: 0.372) > T_{Si} (NSC: 0.035) > L_{bc} (NSC: 0.032) > $T_{S,o}$ (NSC: 0.0063) and the hydraulic performance (ΔP_S) as L_{bc} (NSC: 4.5) > $\dot{m}_S$ (NSC: 3.62).
- The sensitivity of operational cost of STHX for the process and fiscal parameters was observed to be in the following order C_{elec} (NSC: 0.99) > $\dot{m}_S$ (NSC: 0.78) > L_{bc} (NSC: 0.41) > i (NSC: 0.18).
- The parametric analysis showed that an increase in the shell-side flow rate increased the heat transfer coefficient, pressure drop, and pumping power because of enhanced turbulence.

- The shell-side heat transfer coefficient per unit pressure drop decreased with increasing flow rate as well as the number of baffles that indicated a higher-order increase in the pressure drops, which in turn increased the heat exchanger operating cost.
- The heat exchanger operating cost was observed to be a strong function of fiscal parameters, i.e., cost index factor, interest rate, electricity cost, etc. Therefore, the values of these parameters should be selected carefully for reliable cost estimation.
- The exergoeconomic analysis calculated the stream exergy-and-monetary costs. It helped to develop the cost flow diagram. The final hot water production cost was calculated as 2.1 €/h. It is found to increase with increasing flow rates, the number of baffles, and the inflation rate.
- The optimization improved the STHX design appreciably by modifying the design parameters. For the optimal heat exchanger, the heat transfer area reduced by ~26.4%, capital cost by ~20.5%, operational cost by ~50.7%, total expenditure by ~22%, and the stream cost by ~21%.

Acknowledgment

The authors acknowledge the support provided by Khwaja Fareed University of Engineering and Information Technology (KFUEIT), Rahim Yar Khan. Also, Dr. Muhammad Wakil Shahzad acknowledges the support provided by Northumbria University, UK under reference # RDF20/EE/MCE/SHAHZAD. Dr. Syed Zubair would like to acknowledge the support received from King Fahd University of Petroleum & Minerals (KFUPM) through the project IN171048. Also acknowledged is the support provided by Mr. Kashif AllahYar (an undergraduate student at the Mechanical Engineering Department KFUEIT), for organizing the literature and numerical model.

722 **Nomenclature**

A	constant
A	heat transfer area, m^2
B	constant
B_c	baffle cut, %
b_o	constant used in eq. (3)
$\dot{C}$	product cost, (€/h)
C_{total}	total cost of equipment, €
C_o	annual current cost, €/y
C_{ele}	cost of electricity, €/kWh
C_p	specific heat capacity, J/kg.K
D	diameter, m
D_w	hydraulic diameter, m
$\overline{ex}$	specific exergy, k.J/kg
F	friction factor
G	mass flux, $kg/s.m^2$
G_w	mass flux in the window area, $kg/s.m^2$
H	heat transfer coefficient, $W/m^2.K$
h'	enthalpy, kJ
I	interest rate, %
J	the correction factor for the heat transfer coefficient
K	thermal conductivity, W/m.K
K_f	parameter in Appendix A-2
L_{bi}	inlet baffle spacing, m
L_{bo}	outlet baffle spacing, m
L_{bc}	central baffle spacing, m
L_t	tube length, m
$\dot{m}$	flow rate, kg/s
N	flow coefficient, $kg^{-1}.m^{-1}$
n_y	equipment life, year
N_b	number of baffles
N_c	total number of tube rows in cross-flow
Nu	Nusselt number

N_t	total number of tubes
N_p	number of tube passes
p_c	constant in Eq. (4)
P	parameter in Eq. (31)
PP	pumping power, W
Pr	Prandtl number,
P_t	tube pitch, m
ΔP	pressure drop, Pa
R	correction factor for pressure drop
S	entropy, J/K
S	leakage areas, m^2
$\dot{S}_{gen}$	entropy generation rate, W/K
Tb	baffle thickness, m
Re	Reynolds number
R_f	fouling resistance, m^2.K/W
T_{in}	temperature inlet, °C
T_{out}	temperature outlet, °C
U	overall heat transfer coefficient, W/m^2.K
V	velocity, m/s
W	weight, kg
$\dot{W}_p$	pump work, kW
X	exergy, kW
X_D	exergy destruction, kW
$\dot{Z}$	annual rate of capital investment, €/y

Greek Symbols

ζ	rate of fixed cost, €/s
B	layout, deg
ε	effectiveness
θ_{ctl}	angle between centerline and baffle cut, deg
ρ	density, kg/m^3
Φ	viscosity correction factor
μ	viscosity, Pa.s

ψ	is the feed split ration
Λ	operation hours, hour
H	efficiency

Subscripts

0	dead state
A	combined coefficient
bI	ideal tube bundle
B	bypass
C	cross-flow or central baffle spacing
ctl	center-line tube
c,i	cold in
c,o	cold out
Cb	combined coefficient
Cr	cross-flow
E	equivalent or exist baffle
h,i	hot in
h,o	hot out
I	in
L	leakage
M	cross-flow area at the centerline
O	out
P	combined coefficient
R	laminar flow
S	shell
Sb	shell-to-baffle
S	unequal baffle spacing
T	tube
Tb	tube-to-baffle
t,i	tube inside
t,o	tube outside
W	wall or window

Abbreviations

BH	brine heater
CAPC	capital cost

CEPCI	chemical engineering plant cost index
CRF	capital recovery factor
DH	distillate heater
HXs	heat exchangers
OFAT	one-factor-at-a-time
OPC	operational cost
STHX	shell and tube heat exchanger

723

724

725

References

[1] Catrini P, Cipollina A, Micale G, Piacentino A, Tamburini A. Exergy analysis and thermoeconomic cost accounting of a Combined Heat and Power steam cycle integrated with a Multi Effect Distillation- Thermal Vapour Compression desalination plant. Energy Convers Manag 2017;149:950–65.

[2] Chitgar N, Emadi MA, Chitsaz A, Rosen MA. Investigation of a novel multigeneration system driven by a SOFC for electricity and fresh water production. Energy Convers Manag 2019;196:296–310.

[3] Gholizadeh T, Vajdi M, Rostamzadeh H. Exergoeconomic optimization of a new trigeneration system driven by biogas for power, cooling, and freshwater production. Energy Convers Manag 2020;205:112417.

[4] Serth RW, Lestina T. Process Heat Transfer (Second Edition) Principles, Applications and Rules of Thumb. 2014.

[5] Costa ALH, Queiroz EM. Design optimization of shell-and-tube heat exchangers. Appl Therm Eng 2008;28:1798–805. doi:10.1016/j.applthermaleng.2007.11.009.

[6] Gulenoglu C, Akturk F, Aradag S, Uzol NS, Kakac S. Experimental comparison of performances of three different plates for gasketed plate heat exchangers. Int J Therm Sci 2014;75:249–56. doi:10.1016/j.ijthermalsci.2013.06.012.

[7] Rao RV, Patel V. Multi-objective optimization of heat exchangers using a modified teaching-learning-based optimization algorithm. Appl Math Model 2013;37:1147–62. doi:10.1016/j.apm.2012.03.043.

[8] Zhang Z, Ma D, Fang X, Gao X. Experimental and numerical heat transfer in a helically baffled heat exchanger combined with one three-dimensional finned tube. Chem Eng Process Process Intensif 2008;47:1738–43.

[9] Thome JR. Engineering Data Book III. Wolverine Tune, Inc.; 2004.

[10] El Maakoul A, Laknizi A, Saadeddine S, El Metoui M, Zaite A, Meziane M, et al. Numerical comparison of shell-side performance for shell and tube heat exchangers with trefoil-hole, helical and segmental baffles. Appl Therm Eng 2016;109:175–85. doi:10.1016/j.applthermaleng.2016.08.067.

[11] Ambekar AS, Sivakumar R, Anantharaman N, Vivekenandan M. CFD simulation study of shell and tube heat exchangers with different baffle segment configurations. Appl Therm Eng 2016;108:999–1007. doi:10.1016/j.applthermaleng.2016.08.013.

[12] Falav Jozaei A, Baheri A, Hafshejani MK, Arad A. Optimization of baffle spacingon heat transfer, pressure drop and estimated price in a shell-and-tube heat exchanger. World Appl Sci J 2012;18:1727–36. doi:10.5829/idosi.wasj.2012.18.12.2484.

[13] Abdelkader BA, Zubair SM. The effect of a number of baffles on the performance of shell-and-tube heat exchangers. Heat Transf Eng 2019;40:39–52. doi:10.1080/01457632.2017.1404806.

764 [14] Gao B, Bi Q, Nie Z, Wu J. Experimental study of effects of baffle helix angle on shell-side
765 performance of shell-and-tube heat exchangers with discontinuous helical baffles. Exp
766 Therm Fluid Sci 2015;6:48–57, Nov.

767 [15] Abdelkader BA, Jamil MA, Zubair SM. Thermal-Hydraulic Characteristics of Helical
768 Baffle Shell-and-Tube Heat Exchangers. Heat Transf Eng 2019.
769 doi:10.1080/01457632.2019.1611135.

770 [16] Kayabasi E, Kurt H. Simulation of heat exchangers and heat exchanger networks with an
771 economic aspect. Eng Sci Technol an Int J 2018;21:70–6. doi:10.1016/j.jestch.2018.02.006.

772 [17] Roy U, Majumder M. Economic optimization and energy analysis in shell and tube heat
773 exchanger by meta-heuristic approach. Vacuum 2019;166:413–8.
774 doi:10.1016/j.vacuum.2018.12.052.

775 [18] Selbaş R, Kizilkan Ö, Reppich M. A new design approach for shell-and-tube heat
776 exchangers using genetic algorithms from economic point of view. Chem Eng Process
777 Process Intensif 2006;45:268–75. doi:10.1016/j.cep.2005.07.004.

778 [19] Vasconcelos Segundo EH de, Mariani VC, Coelho L dos S. Design of heat exchangers using
779 Falcon Optimization Algorithm. Appl Therm Eng 2019;156:119–44.
780 doi:10.1016/j.applthermaleng.2019.04.038.

781 [20] Bejan A, Tsatsaronis G, Moran M. Thermal Design and Optimization. Wiley; 1996.

782 [21] Lazzaretto A, Tsatsaronis G. SPECO: A systematic and general methodology for calculating
783 efficiencies and costs in thermal systems. Energy 2006;31:1257–89.

784 [22] Keshavarzian S, Rocco M V., Gardumi F, Colombo E. Practical approaches for applying
785 thermoeconomic analysis to energy conversion systems: Benchmarking and comparative
786 application. Energy Convers Manag 2017;150:532–44.

787 [23] Hajabdollahi H, Ahmadi P, Dincer I. Thermoeconomic optimization of a shell and tube
788 condenser using both genetic algorithm and particle swarm. Int J Refrig 2011;34:1066–76.
789 doi:10.1016/j.ijrefrig.2011.02.014.

790 [24] Jamil MA, Zubair SM. Design and analysis of a forward feed multi-effect mechanical vapor
791 compression desalination system : An exergo-economic approach. Energy 2017;140:1107–
792 20. doi:10.1016/j.energy.2017.08.053.

793 [25] Zhang C, Liu C, Wang S, Xu X, Li Q. Thermo-economic comparison of subcritical organic
794 Rankine cycle based on different heat exchanger configurations. Energy 2017;123:728–41.
795 doi:10.1016/j.energy.2017.01.132.

796 [26] Jamil MA, Elmutasim SM, Zubair SM. Exergo-economic analysis of a hybrid
797 humidification dehumidification reverse osmosis (HDH-RO) system operating under
798 different retrofits. Energy Convers Manag 2018;158:286–97.

799 [27] Ghazi M, Ahmadi P, Sotoodeh AF, Taherkhani A. Modeling and thermo-economic
800 optimization of heat recovery heat exchangers using a multimodal genetic algorithm.
801 Energy Convers Manag 2012;58:149–56. doi:10.1016/j.enconman.2012.01.008.

802 [28] Caputo AC, Pelagagge PM, Salini P. Heat exchanger design based on economic
803 optimisation. Appl Therm Eng 2008;28:1151–9.

804 [29] Guo J, Cheng L, Xu M. Optimization design of shell-and-tube heat exchanger by entropy
805 generation minimization and genetic algorithm. Appl Therm Eng 2009;29:2954–60.
806 doi:10.1016/j.applthermaleng.2009.03.011.

807 [30] Guo J, Xu M, Cheng L. The application of field synergy number in shell-and-tube heat
808 exchanger optimization design. Appl Energy 2009;86:2079–87.
809 doi:10.1016/j.apenergy.2009.01.013.

810 [31] Ponce-Ortega JM, Serna-González M, Jiménez-Gutiérrez A. Use of genetic algorithms for
811 the optimal design of shell-and-tube heat exchangers. Appl Therm Eng 2009;29:203–9.
812 doi:10.1016/j.applthermaleng.2007.06.040.

813 [32] Patel VK, Rao R V. Design optimization of shell-and-tube heat exchanger using particle
814 swarm optimization technique. Appl Therm Eng 2010;30:1417–25.
815 doi:10.1016/j.applthermaleng.2010.03.001.

816 [33] Şencan Şahin A, Kiliç B, Kiliç U. Design and economic optimization of shell and tube heat
817 exchangers using Artificial Bee Colony (ABC) algorithm. Energy Convers Manag
818 2011;52:3356–62. doi:10.1016/j.enconman.2011.07.003.

819 [34] Hadidi A, Hadidi M, Nazari A. A new design approach for shell-and-tube heat exchangers
820 using imperialist competitive algorithm (ICA) from economic point of view. Energy
821 Convers Manag 2013;67:66–74. doi:10.1016/j.enconman.2012.11.017.

822 [35] Hadidi A, Nazari A. Design and economic optimization of shell-and-tube heat exchangers
823 using biogeography-based (BBO) algorithm. Appl Therm Eng 2013;51:1263–72.
824 doi:10.1016/j.applthermaleng.2012.12.002.

825 [36] Asadi M, Song Y, Sunden B, Xie G. Economic optimization design of shell-and-tube heat
826 exchangers by a cuckoo-search-algorithm. Appl Therm Eng 2014;73:1032–40.
827 doi:10.1016/j.applthermaleng.2014.08.061.

828 [37] Sadeghzadeh H, Ehyaei MA, Rosen MA. Techno-economic optimization of a shell and tube
829 heat exchanger by genetic and particle swarm algorithms. Energy Convers Manag
830 2015;93:84–91. doi:10.1016/j.enconman.2015.01.007.

831 [38] Khosravi R, Khosravi A, Nahavandi S, Hajabdollahi H. Effectiveness of evolutionary
832 algorithms for optimization of heat exchangers. Energy Convers Manag 2015;89:281–8.
833 doi:10.1016/j.enconman.2014.09.039.

834 [39] Mohanty DK. Application of firefly algorithm for design optimization of a shell and tube
835 heat exchanger from economic point of view. Int J Therm Sci 2016;102:228–38.
836 doi:10.1016/j.ijthermalsci.2015.12.002.

837 [40] Hajabdollahi H, Naderi M, Adimi S. A comparative study on the shell and tube and gasket-
838 plate heat exchangers: The economic viewpoint. Appl Therm Eng 2016;92:271–82.

839 [41] Dhavle S V., Kulkarni AJ, Shastri A, Kale IR. Design and economic optimization of shell-
840 and-tube heat exchanger using cohort intelligence algorithm. Neural Comput Appl

2018;30:111–25. doi:10.1007/s00521-016-2683-z.

[42] Wen J, Yang H, Jian G, Tong X, Li K, Wang S. Energy and cost optimization of shell and tube heat exchanger with helical baffles using Kriging metamodel based on MOGA. Int J Heat Mass Transf 2016;98:29–39, Jul.

[43] Rao RV, Saroj A. Constrained economic optimization of shell-and-tube heat exchangers using elitist-Jaya algorithm. Energy 2017;128:785–800. doi:10.1016/j.energy.2017.04.059.

[44] Vasconcelos Segundo EH de, Amoroso AL, Mariani VC, Coelho L dos S. Economic optimization design for shell-and-tube heat exchangers by a Tsallis differential evolution. Appl Therm Eng 2017;111:143–51. doi:10.1016/j.applthermaleng.2016.09.032.

[45] Tharakeshwar TK, Seetharamu KN, Durga Prasad B. Multi-objective optimization using bat algorithm for shell and tube heat exchangers. Appl Therm Eng 2017;110:1029–38. doi:10.1016/j.applthermaleng.2016.09.031.

[46] Mirzaei M, Hajabdollahi H, Fadakar H. Multi-objective optimization of shell-and-tube heat exchanger by constructal theory. Appl Therm Eng 2017;125:9–19. doi:10.1016/j.applthermaleng.2017.06.137.

[47] Iyer VH, Mahesh S, Malpani R, Sapre M, Kulkarni AJ. Adaptive Range Genetic Algorithm: A hybrid optimization approach and its application in the design and economic optimization of Shell-and-Tube Heat Exchanger. Eng Appl Artif Intell 2019;85:444–61. doi:10.1016/j.engappai.2019.07.001.

[48] Sai JP, Rao BN. Efficiency and economic optimization of shell and tube heat exchanger using bacteria foraging algorithm. SN Appl Sci 2020;2:1–7. doi:10.1007/s42452-019-1798-0.

[49] Sinnot R, Towler G. Chemical Engineering Design. 2nd ed. 1993.

[50] Fraas AP. Heat Exchanger Design. New York: John Wiley & Sons; 1989.

[51] Peters MS, Timmerhaus KD. Plant Design and Economics for Chemical Engineers. 4th ed. McGraw-Hill; 1991.

[52] Kern DQ. Process Heat Transfer. McGraw-Hill; 1950.

[53] Palen JW, Taborek J. Solution of shell side flow pressure drop and heat transfer by stream analysis method, Chem. Eng. Prog. Symp. Ser., vol. 65, no. 93, pp. 53-63. 1969.

[54] Tsatsaronis G. Definitions and nomenclature in exergy analysis and exergoeconomics. Energy 2007;32:249–53.

[55] Fitzsimons L, Corcoran B, Young P, Foley G. Exergy analysis of water purification and desalination: A study of exergy model approaches. Desalination 2015;359:212–24.

[56] Sharqawy MH, Lienhard V JH, Zubair SM. Thermophysical properties of seawater: a review of existing correlations and data. Desalin Water Treat 2010;16:354–80.

[57] Sharqawy MH, Lienhard V JH, Zubair SM. On exergy calculations of seawater with applications in desalination systems. Int J Therm Sci 2011;50:187–96.

878 [58] Nayar KG, Sharqawy MH, Banchik LD, Lienhard V JH. Thermophysical properties of
879 seawater: A review and new correlations that include pressure dependence. Desalination
880 2016;390:1–24.

881 [59] El-Sayed YM. The Thermoeconomics of Energy Conversions. Amsterdam: Elsevier; 2003.

882 [60] El-Sayed YM. Designing desalination systems for higher productivity. Desalination
883 2001;134:129–58.

884 [61] Shabani MR, Yekta RB. Chemical processes equipment cost estimation using parametric
885 models. Cost Eng 2006;48:26–32.

886 [62] Turton R, Bailie RC, Whiting WB, Shaeiwitz JA, Bhattacharyya D. Analysis, Synthesis,
887 and Design of Chemical Processes. 4th ed. Old Tappan, NJ, USA: Prentis Hall; 2013.

888 [63] Li YR, Du MT, Wu CM, Wu SY, Liu C, Xu JL. Economical evaluation and optimization
889 of subcritical organic Rankine cycle based on temperature matching analysis. Energy
890 2014;68:238–47.

891 [64] Fettaka S, Thibault J, Gupta Y. Design of shell-and-tube heat exchangers using
892 multiobjective optimization. Int J Heat Mass Transf 2013;60:343–54.

893 [65] Li J, Yang Z, Hu S, Yang F, Duan Y. Effects of shell-and-tube heat exchanger arranged
894 forms on the thermo-economic performance of organic Rankine cycle systems using
895 hydrocarbons. Energy Convers Manag 2020;203:112248.
896 doi:10.1016/j.enconman.2019.112248.

897 [66] Hall SG, Ahmad S, Smith R. Capital cost targets for heat exchanger networks comprising
898 mixed materials of construction, pressure ratings and exchanger types. Comput Chem Eng
899 1990;14:319–35.

900 [67] Taal M, Bulatov I, Kleme J, Stehl P. Cost estimation and energy price forecasts for
901 economic evaluation of retrofit projects. Appl Therm Eng 2003;23:1819–35.

902 [68] Sanaye S, Hajabdollahi H. Multi-objective optimization of shell and tube heat exchangers.
903 Appl Therm Eng 2010;30:1937–45. doi:10.1016/j.applthermaleng.2010.04.018.

904 [69] Azad AV, Amidpour M. Economic optimization of shell and tube heat exchanger based on
905 constructal theory. Energy 2011;36:1087–96. doi:10.1016/j.energy.2010.11.041.

906 [70] Loh HP, Lyons J, White CW. Process Equipment Cost Estimation, Final Report. 2002.

907 [71] Tremblay PW-, Gosselin L. Minimizing shell-and-tube heat exchanger cost with genetic
908 algorithms and considering maintenance. Int J Energy Res 2007;31:867–85.

909 [72] Rao RV, Saroj A. Economic optimization of shell-and-tube heat exchanger using Jaya
910 algorithm with maintenance consideration. Appl Therm Eng 2017;116:473–87.
911 doi:10.1016/j.applthermaleng.2017.01.071.

912 [73] Caputo AC, Pelagagge PM, Salini P. Manufacturing cost model for heat exchangers
913 optimization. Appl Therm Eng 2016;94:513–33.
914 doi:10.1016/j.applthermaleng.2015.10.123.

915 [74] Vatavuk WM. Updating the Cost Index. Chem Eng 2002:62–70.

916 [75] Jenkins S. 2019 Chemical engineering plant cost index annual average 2020.
917 https://www.chemengonline.com/2019-chemical-engineering-plant-cost-index-annual-
918 average/ (accessed April 9, 2020).

919 [76] Jamil MA, Zubair SM. On thermoeconomic analysis of a single-effect mechanical vapor
920 compression desalination system. Desalination 2017;420:292–307.

921 [77] Jamil MA, Zubair SM. Effect of feed flow arrangement and number of evaporators on the
922 performance of multi-effect mechanical vapor compression desalination systems.
923 Desalination 2018;429:76–87.

924 [78] Nafey AS, Fath HES, Mabrouk AA. Exergy and thermoeconomic evaluation of MSF
925 process using a new visual package. Desalination 2006;201:224–40.

926 [79] Mabrouk AA, Nafey AS, Fath HES. Thermoeconomic analysis of some existing
927 desalination processes. Desalination 2007;205:354–73.

928 [80] El-Emam RS, Dincer I. Thermodynamic and thermoeconomic analyses of seawater reverse
929 osmosis desalination plant with energy recovery. Energy 2014;64:154–63.

930 [81] Rosen M a. A concise review of exergy-based cconomic methods. Int. Conf. Energy
931 Environ., 2008, p. 9.

932 [82] Qureshi BA, Zubair SM. A comprehensive design and rating study of evaporative coolers
933 and condensers. Part II. Sensitivity analysis. Int J Refrig 2006;29:659–68.

934 [83] Kitchell JF, Stewart DJ, Weininger D. Applications of a Bioenergetics Model to Yellow
935 Perch (Perca flavescens) and Walleye (Stizostedion vitreum vitreum). J Fish Res Board
936 Canada 1977;34:1922–35.

937 [84] Hussaini IS, Zubair SM, Antar MA. Area allocation in multi-zone feedwater heaters. Energy
938 Convers Manag 2007;48:568–75. doi:10.1016/j.enconman.2006.06.003.

939 [85] Kim JH, Simon TW. Journal of heat transfer policy on reporting uncertainties in
940 experimental measurements and results. J Heat Transfer 1993;115:5–6.
941 doi:10.1115/1.2910670.

942 [86] Taylor BN, Kuyatt CE. Guidelines for evaluating and expressing the uncertainty of NIST
943 measurement results, Gaithersburg, MD, U.S. Departmente of Commerce, Technology
944 Administration, National Institute of Standards and Technology. 1994.

945 [87] Masi M, Fogliani S, Carrà S. Sensitivity analysis on indium phosphide liquid encapsulated
946 Czochralski growth. Cryst Res Technol 1999;34:1157–67.

947 [88] James CA, Taylor RP, Hodge BK. The application of uncertainty analysis to cross-flow heat
948 exchanger performance predictions. Heat Transf Eng 1995;16:50–62.

949 [89] James CA, Taylor RP, Hodge BK. Analysis and design of energy systems. 3rd ed. Prentice
950 Hall, Englewood Cliffs, NJ; 1998.

951 [90] Serth RW. Process Heat Transfer- Principles and Application. 1st ed. Amsterdem: Elsevier

952 Science and Technology Books; 2007.

953 [91] Jamil MA, Din ZU, Goraya TS, Yaqoob H, Zubair SM. Thermal-hydraulic characteristics
954 of gasketed plate heat exchangers as a preheater for thermal desalination systems. Energy
955 Convers Manag 2020;205:112425.

956 [92] Jamil MA, Shahzad MW, Zubair SM. A comprehensive framework for thermoeconomic
957 analysis of desalination systems. Energy Convers Manag 2020;222:113188.

958

959

Appendix: Tables for correction factors, constants, and coefficients for Bell-Delaware and Wills-Johnston methods

Table A.1.

Empirical coefficients for j_i and f_i [9]

Layout	Re	a_1	a_2	a_3	a_4	b_1	b_2	b_3	b_4
	10^5-10^4	0.321	-0.388	1.450	0.519	0.372	-0.123	7.00	0.500
	10^4-10^3	0.321	-0.388			0.486	-0.152		
30°	10^3-10^2	0.593	-0.477			4.570	-0.476		
	10^2-10	1.360	-0.657			45.10	-0.973		
	<10	1.400	-0.667			48.00	-1.00		
	10^5-10^4	0.370	-0.396	1.930	0.500	0.303	-0.126	6.59	0.520
	10^4-10^3	0.370	-0.396			0.333	-0.136		
45°	10^3-10^2	0.730	-0.500			3.500	-0.476		
	10^2-10	0.498	-0.656			26.20	-0.913		
	<10	1.550	-0.667			32.00	-1.00		
	10^5-10^4	0.370	-0.395	1.187	0.370	0.391	-0.148	6.30	0.378
	10^4-10^3	0.107	-0.266			0.0815	+0.022		
90°	10^3-10^2	0.408	-0.460			6.090	-0.602		
	10^2-10	0.900	-0.631			32.10	-0.963		
	<10	0.970	-0.667			35.00	-1.00		

965 **Table A.2.**

966 Bell Delaware methods correction factors for calculation of shell side heat transfer coefficient [9].

Correction factor	Accounts for	Governing equation
Baffle window flow CF (J_c)	Non-ideal cross-flow through the window zone	$J_C = 0.55 + 0.72\,(1 - 2F_w)$ $F_w = (\theta_{ctl}/360) - (\sin\theta_{ctl}/2\pi),\ \theta_{ctl} = 2\cos^{-1}\left((D_s/D_{ctl})(1-2(B_c/100))\right)$
Baffle leakage CF (J_L)	Flow-through the gaps between the baffle and shell, and the baffle and tube diameter	$J_L = 0.44\left(1-\frac{S_{sb}}{S_{sb}+S_{tb}}\right)+\left[1-0.44\left(1-\frac{S_{sb}}{S_{sb}+S_{tb}}\right)\right]\exp\left(-2.2\frac{S_{sb}+S_{tb}}{S_m}\right)$ $S_{sb} = 0.00436 D_s L_{sb}(360-\theta_{ds}),\ S_{tb} = \left\{\pi/4\left[(D_t+L_{tb})^2\right]\right\} N_t(1-F_w)$ $S_m = L_{bc}\left[L_{bb}+\left((D_{ctl}/L_{tp,eff})(L_{tp}-D_t)\right)\right],\ \theta_{ds} = 2\cos^{-1}\left[1-2(B_c/100)\right]$
Tube bundle bypass CF (J_B)	Flows through bypass areas due to the gap between the shell wall and tube bundle	$J_B = \exp\left[-C_{bh}\,F_{sbp}\left(1-\sqrt[3]{2r_{ss}}\right)\right]$ $F_{sbp} = \frac{S_b}{S_m},\ S_b = L_{bc}\left[(D_s - D_{otl}) + L_{pl}\right],\ r_{ss} = N_{ss}\Big/\left((D_s/L_{pp})(1-2(B_c/100))\right)$
Unequal baffle spacing CF (J_S)	The difference in inlet and outlet baffle spacing compared to the central ones	$J_S = \frac{(N_b-1)+(L_{bi}/L_{bc})^{1-n}+(L_{bo}/L_{bc})^{1-n}}{(N_b-1)+(L_{bi}/L_{bc})+(L_{bo}/L_{bc})}$
Laminar flow CF (J_R)	The adverse temperature gradient formed in the boundary layer.	$J_R = (10/N_c)^{0.18}+\left((20-\mathrm{Re})/80\right)\left[(10/N_c)^{0.18}-1\right]$ $N_c = (N_{tcc}+N_{tcw})(N_b+1),\ N_{tcw} = 0.8/L_{pp}\left[D_s(B_c/100)-\left((D_s-D_{ctl})/2\right)\right]$
Wall viscosity (J_μ)	The variation in fluid properties between the bulk and the wall	$J_\mu = (\mu/\mu_{wall})^m\ \widehat{U}_Y = \frac{dY}{dX}\widehat{U}_X$

967

Table A.3.

Flow coefficients for flow stream analysis (Wills-Johnston) method [1].

Coefficient	Governing equation	Description
Combined flow coefficient (n_p, n_a , n_{cb})	$n_p = 1/\left(n_a^{-0.5} + n_s^{-0.5} + n_t^{-0.5}\right)^2$ $n_a = n_w + n_{cb}$, $n_{cb} = 1/\left(n_c^{-0.5} + n_b^{-0.5}\right)^2$	The effect of different resistance coefficient over ΔP and h.
Shell-to-baffle leakage resistance coefficient (n_s)	$n_s = \dfrac{0.036(t_b/\delta_{sb}) + 2.3(t_b/\delta_{sb})^{-0.177}}{2\rho S_s^{\,2}}$ where $S_s = \pi(D_s - \delta_{sb})\delta_{sb}$	Shell-to-baffle flow resistance due to clearance between shell-to-baffle.
Tube-to-baffle clearance resistance coefficient (n_t)	$n_t = \dfrac{0.036(t_b/\delta_{tb}) + 2.3(t_b/\delta_{sb})^{-0.177}}{2\rho S_t^{\,2}}$ where $S_t = N_T\pi(D_s + \delta_{st})\delta_{st}$	Tube-to-baffle flow resistance due to clearance between tube-to-baffle.
Window flow resistance coefficient (n_w)	$n_w = \dfrac{1.9\exp(0.6856\,S_w/S_w)}{2\,\rho\,S_w^{\,2}}$	Due to mix the flow of cross and combine bypass flow.
Bypass flow resistance coefficient (n_b)	$n_b = \dfrac{a(D_s - 2L_c)/P_{TP} + N_{ss}}{2\rho S_b^{\,2}}$ where $S_b = (2\delta_{by}\,D_s + \delta_{pp})L_B$	The combined effect of the bundle and pass partition bypass streams.
Cross-flow resistance coefficient (n_c)	$n_c = \dfrac{N_c K_f}{2\rho S_m^{\,2}}$ $K_f = 0.272 + \dfrac{0.207\text{x}10^3}{\text{Re}} + \dfrac{0.102\text{x}10^3}{\text{Re}^2} - \dfrac{0.286\text{x}10^3}{\text{Re}^3}$ for $3 < \text{Re} < 2\text{x}10^3$ $K_f = 0.267 + \dfrac{0.249\text{x}10^4}{\text{Re}} - \dfrac{0.927\text{x}10^7}{\text{Re}^2} + \dfrac{0.10\text{x}10^{11}}{\text{Re}^3}$ for $2\text{x}10^3 < \text{Re} < 2\text{x}10^6$	Obtained from the ideal bank correction factor and a function of cross-flow Reynold number. The parameter K_f, for in-line square arrays.